SEMARAK ILMU PUBLISHING

Journal of Advanced Research in Applied Mechanics

Journal homepage:
https://semarakilmu.com.my/journals/index.php/appl_mech/index
ISSN: 2289-7895

An Experimental Study on the Mechatronics Design and Implementation of an Intelligent Active Vibration Control System for a CSLRFM

Abbas Moloody[1,*], Azizan As'arry[1], Tang Sai Hong[1], Raja Kamil[2], Mohd Zarhamdy Md. Zain[3], Irfan Bahiuddin[4]

[1] Department of Mechanical and Manufacturing Engineering, Faculty of Engineering, Universiti Putra Malaysia (UPM), 43400 Serdang, Selangor, Malaysia
[2] Department of Electrical and Electronics Engineering, Faculty of Engineering, Universiti Putra Malaysia (UPM), 43400 Serdang, Selangor, Malaysia
[3] Department of Applied Mechanics and Design, Faculty of Engineering, Universiti Teknologi Malaysia (UTM), 54100 Kuala Lumpur, Malaysia
[4] Department of Mechanical Engineering, Vocational College, Universitas Gadjah Mada, Yogyakarta, Indonesia

ARTICLE INFO

Article history:
Received 19 January 2025
Received in revised form 22 February 2025
Accepted 1 March 2025
Available online 30 March 2025

Keywords:
Mechatronics design; Modified Differential Evolutionary Optimization Algorithm (MDEOA); Intelligent Active Vibration Control (IAVC); Combined Single-Link Robotics Flexible Manipulator (CSLRFM)

ABSTRACT

This study enhances Robotics Flexible Manipulator (RFM) performance by developing a dynamic Mechatronics Test Rig System (MTRS) and a controller for a Combined Single-Link Robotics Flexible Manipulator (CSLRFM). RFMs offer benefits such as lighter weight and faster response but present challenges in motion and vibration control under disturbances. To address this, a Modified Differential Evolution Optimization Algorithm (MDEOA) tunes a PID controller to improve vibration suppression. Additionally, a New Gyroscopic Combined Actuator (NGCA) is introduced for Intelligent Active Vibration Control (IAVC). Comparing (AVC-DEO-PID) and (AVC-FL-PID) controllers with traditional PID, Fuzzy, and (Fuzzy-PID) controllers, the results show (AVC-DEO-PID) performs best, achieving up to about 93.471% faster rise and settling times, eliminating maximum overshoot, and reducing steady-state error by about 90-100%. It is 49-78% faster in peak time, with a 92% reduction in settling time, and shows 90-100% consistency across simulations and experiments. The modified algorithm demonstrates its potential in optimizing CSLRFM performance, making it a robust solution for real-time applications.

1. Introduction

This study investigates the optimization and control of mechanical vibrations in a Combined Single-Link Robotics Flexible Manipulator (CSLRFM) using a Modified Differential Evolutionary Optimization Algorithm (MDEOA). The Introduction section has been revised and subdivided into five subsections: Background, Problem Formulation, Literature Survey, Scope and Contribution, and Paper Organization.

[*] *Corresponding author.*
E-mail address: a.moloody@gmail.com; zizan@upm.edu.my

https://doi.org/10.37934/aram.134.1.6189

1.1 Background

Robotic Flexible Manipulators (RFMs) are widely used in industrial applications, including aerospace, manufacturing, and medical robotics, due to their lightweight structure and high operational speed. However, their flexibility introduces significant challenges in controlling vibrations, which can reduce precision, stability, and overall performance. Active Vibration Control (AVC) has emerged as a solution, where advanced control strategies, such as PID controllers, are employed to mitigate vibrations effectively. This study investigates Intelligent Active Vibration Control (IAVC) using innovative control algorithms and actuator designs to address these challenges [1-14].

1.2 Formulation of the Problem

Controlling mechanical vibrations in RFMs presents several challenges, such as managing high degrees of freedom, coupling dynamics, and nonlinearity. Traditional control methods often fail to provide robust solutions under varying operational conditions. Furthermore, designing a system that integrates a gyroscopic actuator with a PID controller optimized through a Modified Differential Evolutionary Optimization Algorithm (MDEOA) introduces complexity in modelling, parameter tuning, and validation. This research focuses on overcoming these challenges by developing an innovative control approach capable of addressing these dynamic complexities [1-14].

1.3 Literature Survey

Numerous studies have explored vibration suppression in RFMs. Traditional PID controllers have been employed for basic control, but their performance declines in nonlinear and dynamic environments. Advanced optimization algorithms, such as Genetic Algorithms (GAs) and Particle Swarm Optimization (PSO), have shown potential for parameter tuning but often suffer from slower convergence and local optima issues. Gyroscopic actuators have been studied for their vibration-damping capabilities but remain underexplored when combined with optimized controllers. This study bridges these gaps by integrating a Modified Differential Evolutionary Optimization Algorithm (MDEOA) with PID control and a New Gyroscopic Combined Actuator (NGCA), offering a novel solution to enhance vibration control [1-14].

1.4 Scope and Contribution

The proposed research distinguishes itself by introducing MDEOA, which utilizes a Strictly Bearish Distributed Exponential Function (SBDEF) to refine mutation and crossover parameters dynamically. This method significantly outperforms traditional optimization algorithms in vibration suppression. Additionally, the study develops a Combined Single-Link Robotics Flexible Manipulator (CSLRFM) equipped with an NGCA to test and validate the proposed control approach. The integration of simulation and experimental analysis ensures comprehensive evaluation, setting this research apart from existing literature.

1.5 Organization of the Paper

The remainder of the paper is organized as follows. Section 2 presents the methodology, including the details of the Modified Differential Evolution Optimization Algorithm (MDEOA) and its application in PID controller tuning. Section 3 discusses simulation and experimental results, comparing the performance of (AVC-DEO-PID) and traditional controllers. Section 4 concludes the paper, highlighting the study's contributions, limitations, and future research directions.

The research introduces the Modified Differential Evolutionary Optimization Algorithm (MDEOA), which incorporates a Strictly Bearish Distributed Exponential Function (SBDEF) to improve PID controller tuning for vibration control in robotic flexible manipulators. Additionally, the integration of the New Gyroscopic Combined Actuator (NGCA) for intelligent active vibration control (IAVC) is a novel aspect of the study. These advancements offer significant improvements over traditional control algorithms, providing better performance in both simulations and experiments. The scientific relevance of this work is emphasized through its contribution to addressing critical gaps in vibration control for robotics, offering a more efficient solution compared to existing methods which compares the proposed method with current approaches and discusses its advantages.

2. Methodology

2.1 Modified Differential Evolution Optimization Algorithm

The Modified Differential Evolution Optimization Algorithm (MDEOA) enhances the traditional Differential Evolution (DE) method by introducing dynamic mutation strategies, self-adaptive control parameters, and adaptive mutation rates to improve convergence and performance in complex optimization problems, Figure 1 shows the flowchart of MDEOA and other factors, [13]. Since its introduction by Das and Suganthan in 2011, MDEOA has been applied successfully across various disciplines. This research adapts MDEOA to optimize PID controller settings for intelligent active vibration control in robotics, utilizing dynamic adjustments in mutation and crossover factors to refine the optimization process, [13]. The method involves defining the optimization problem, modelling the system with partial differential equations, and using MDEOA to iteratively find optimal PID gains that minimize objective functions related to vibration suppression and energy efficiency [15-19].

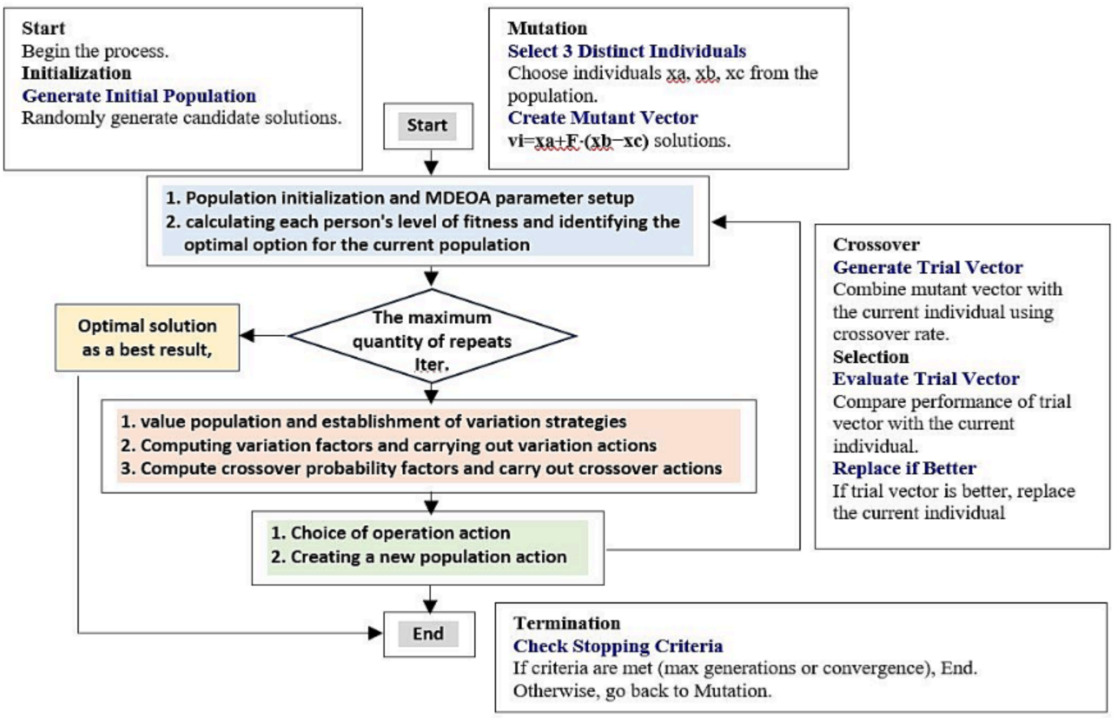

(a)

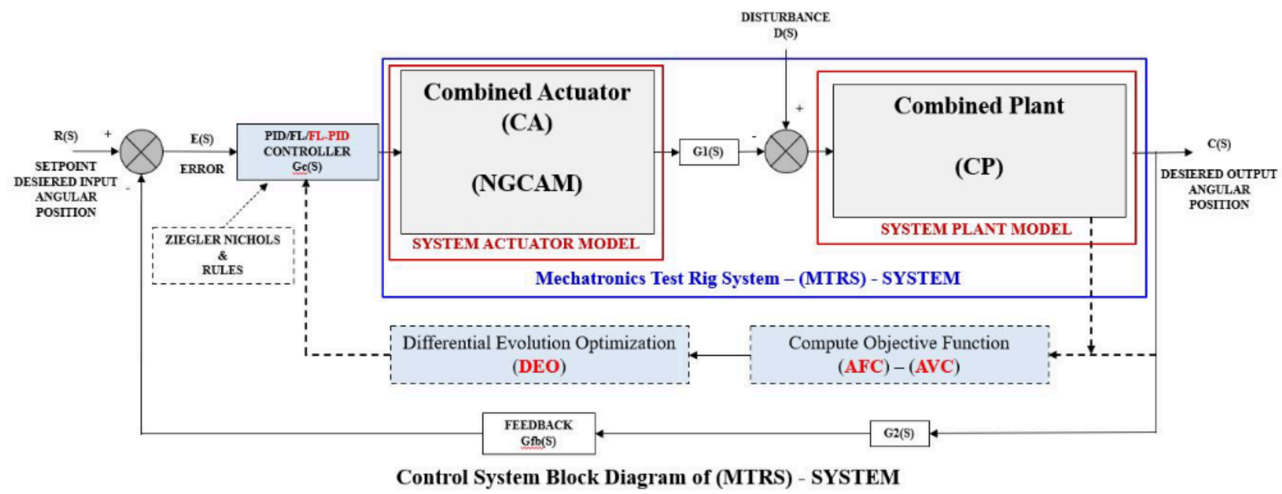

(b)

Fig. 1. (a) Flowchart of MDEOA (b) Control system block diagram of MTRS

2.2 Mutation, Variance Factor and Crossover Scheme Modifications

To balance local exploitation and global search capabilities, this study modifies the mutation scheme of MDEOA by combining DE/rand/1 and DE/best/2 strategies, adjusting the proportion of each strategy to improve convergence speed, Eqs. (1)-(3). The crossover probability factor (C_R) here as Eta (ŋ) is dynamically adjusted to maintain effective search and prevent premature convergence, with (ŋ) increasing, Eq. (4), and Eq. (5), and the F, Variance Factor (VF) here as scaling factor N(K), Eq. (6), decreasing over iterations. The N(K) is recalculated based on the current iteration count to enhance the algorithm's adaptability, [13]. This approach addresses genetic algorithm limitations by ensuring each response has an equal chance of selection, leveraging mutation and crossover operators to iteratively refine solutions and converge on optimal results, [20-30].

$$DE/rand/1 = M_1(time+1) = \Big[N(K)^*\big[\big(x_2(time) - x_3(time)\big)\big]\Big] + [x_1(time)] \quad (1)$$

$$DE/best/1 = M_2(time+1) = \Big[N(K)^*\big[\big(x_1(time) - x_2(time)\big)\big]\Big] + [xbest(time)] \quad (2)$$

$$M_{New}(time+1) = \Big[[(1-\ [\zeta])]^*[[M_2\ (time+1)] + [\epsilon * randn]]\Big] + [[\zeta]^*[[M_1(time+1)] + [\epsilon^* randn]]] \quad (3)$$

$$R(K)\ =\ e^{-\left[\left[\frac{1-K}{[K_m-1]}\right]^*\left[1+\left[\frac{K}{K_m}\right]\right]\right]} \quad (4)$$

$$N(K)\ =\ \left[\left[\left[\frac{1}{\left[1+\left[\beta\cdot e^{-\zeta\cdot\left[\frac{[K-Kmax]}{2}\right]}\right]\right]\times[2Nave]}\right] + N_{min}\right][R(K)]\right] \quad (5)$$

$$ŋ\ = ŋ_{min} + \left[\frac{ŋ_{max} - ŋ_{min}}{1+e^{-a\cdot(K-K_{max})}}\right] \quad (6)$$

Here, key parameters include ζ (damping ratio), N_{max} (maximum scaling factor), N_{min} (minimum scaling factor), and N_{ave} (average scaling factor). Gains or gravitational constants, K, may vary as K_{max} (maximum gains) or K_m (general gains). Noise is denoted by ϵ*randn. Iteration parameters include K (iteration count), K_{max} (maximum iteration count), and K_m (general iteration count). The introduction of noise into the mutation strategy enhances exploration by enabling the algorithm to avoid premature convergence to suboptimal solutions. The non-linear adaptation from the sigmoid function, applied in both crossover probability and scaling factor, facilitates smoother transitions in the optimization process. By combining DE/best/1 and DE/rand/1 with added noise, the method achieves a balanced exploration and exploitation, crucial for fast convergence while avoiding local optima. Here, in Figure 6 (sub-topic 3.1), runs test 5 is notable for its long-term stability and robust control, characterized by a high integral gain (k_I) value that ensures optimal stability and minimizes steady-state errors. The minimization of proportional gain (k_P) and derivative gain (k_D) further reduces the likelihood of oscillations and overshoots, resulting in a well-tuned control system that balances initial stabilization with long-term accuracy.

In the Eqs. (1) to (6), the coefficients α (Alpha), β (Beta), and ϵ (Epsilon) play significant roles in modifying the differential evolution (DE) algorithm. The coefficient (α) adjusts the crossover probability in Eq. (6), where a higher value can lead to more abrupt changes. Similarly, (β), in Eq. (5), adjusts the variance factor, with larger values smoothing the adjustment curve. The coefficient (ϵ) introduces Gaussian noise in Eq. (3) adding stochasticity that enhances exploration. Recommended ranges suggest (α) typically falls between 0.5 and 2.0, (β) between 0.1 and 0.5, and (ϵ) from 0.1 to 1.0, which are randomly varied within their specified ranges respectively with rand () generating a random number within the specified ranges depending on the problem scale and desired exploration-exploitation trade-off. In Figure 1(a), it outlines the process of the Modified Differential Evolutionary Optimization Algorithm (MDEOA). It begins with initializing the population by randomly generating candidate solutions.

In the mutation step, three distinct individuals are selected from the population, and a mutant vector is created by computing differences between them. The crossover step combines the mutant vector with the current individual to form a trial vector, which is then evaluated for performance. If the trial vector performs better, it replaces the current individual. The population's fitness is evaluated, and mutation and crossover factors are adjusted accordingly. The algorithm then checks if the stopping criteria, such as convergence or the maximum number of generations, are met. If not, it returns to mutation, continuing the iterative process until the optimal solution is found. In Figure 1(b), the dotted line leading from the Combined Plant (CP) represents the feedback signal. This feedback is used to measure the output of the system, which is then fed back into the control system for comparison with the setpoint (desired angular position). As the key difference between the dotted line and the solid line, dotted line, represents the feedback path, which carries the actual output from the Combined Plant (CP) to be compared with the desired input and the solid line, represents the forward path, carrying the input signal, controller output, and signals passed through the system components, ultimately affecting the system's actuator and plant. Thus, the dotted line reflects the output feedback used for error calculation and control adjustments, while the solid lines represent the signal flow through the system components, including the controller and actuator.

In Figure 2(a) to 2(b), the x-axis represents the status of parameter changes ($k_P/k_I/k_D$), which likely refers to the scaling or adjustments made to the proportional (k_P), integral (k_I), and derivative (k_D) coefficients of a controller. The units for this axis are dimensionless, as it shows the change in values relative to the initial ones. The y-axis shows parameter values in scientific notation (e.g., 4.54E-01, 1.83E+00, etc.), which likely represents the magnitude of the parameter after tuning, also in dimensionless units, as it refers to the magnitude of the PID controller parameters.

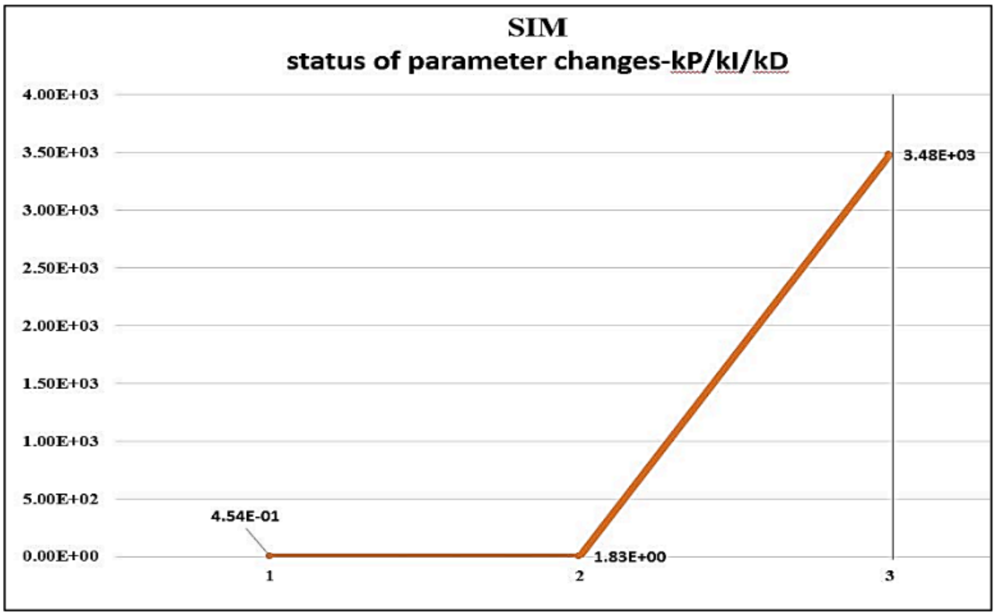

(a)

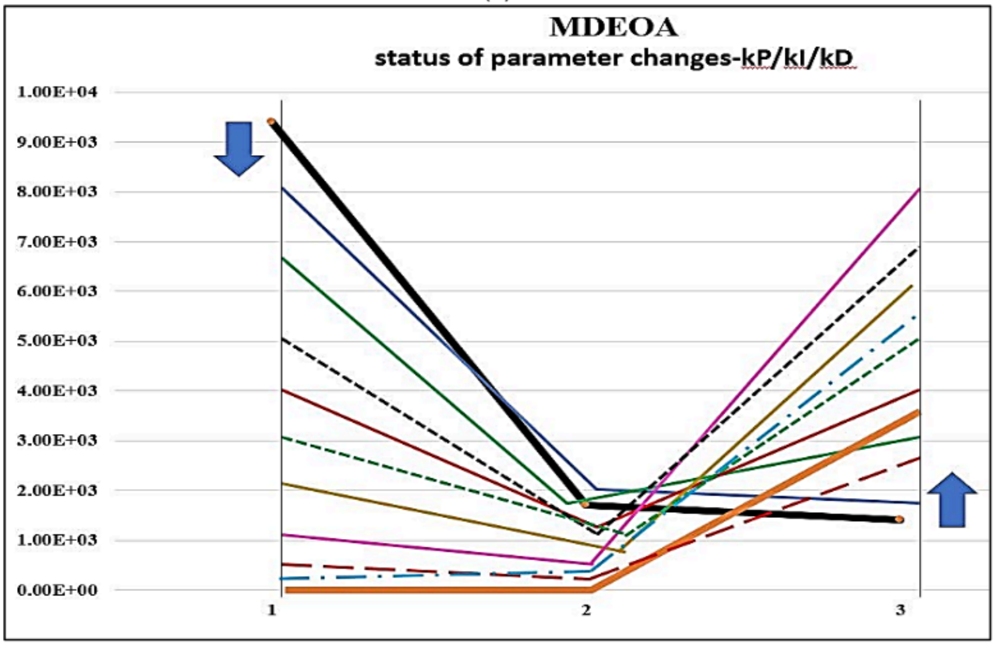

(b)

Fig. 2. (a) Optimized PID parameters $k_P/k_I/K_d$ in SIM (b) PID parameters $k_P/k_I/K_d$ changes strategy in MDEOA

2.3 CAD Design and Development of MTRS

The experimental study and mechatronics design of the MTRS are shown in Figure 3. A CAD drawing has been developed to further clarify the design specifications and support the development process by providing a comprehensive representation of the final design. This CAD drawing also streamlines the material selection and costing methods for the project. Figure 4 presents the front, top, right side, and isometric views of the MTRS design, incorporating the selected materials and also provides the front, top, right side, and isometric views of the New Gyroscopic Combined Actuator Model (NGCAM), detailing components. The design underwent multiple modifications and testing stages before reaching the finalized form. Gyroscope and accelerometer sensors are employed to monitor and manage mechanical vibrations in the RFM. Details of the experimental setup are discussed in the following section.

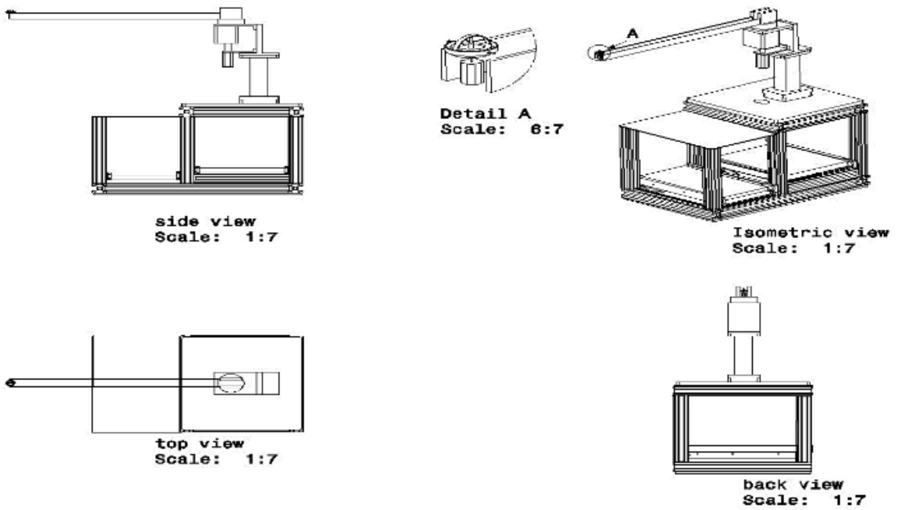

Fig. 3. The front, top, right side, and isometric drawing of the MTRS

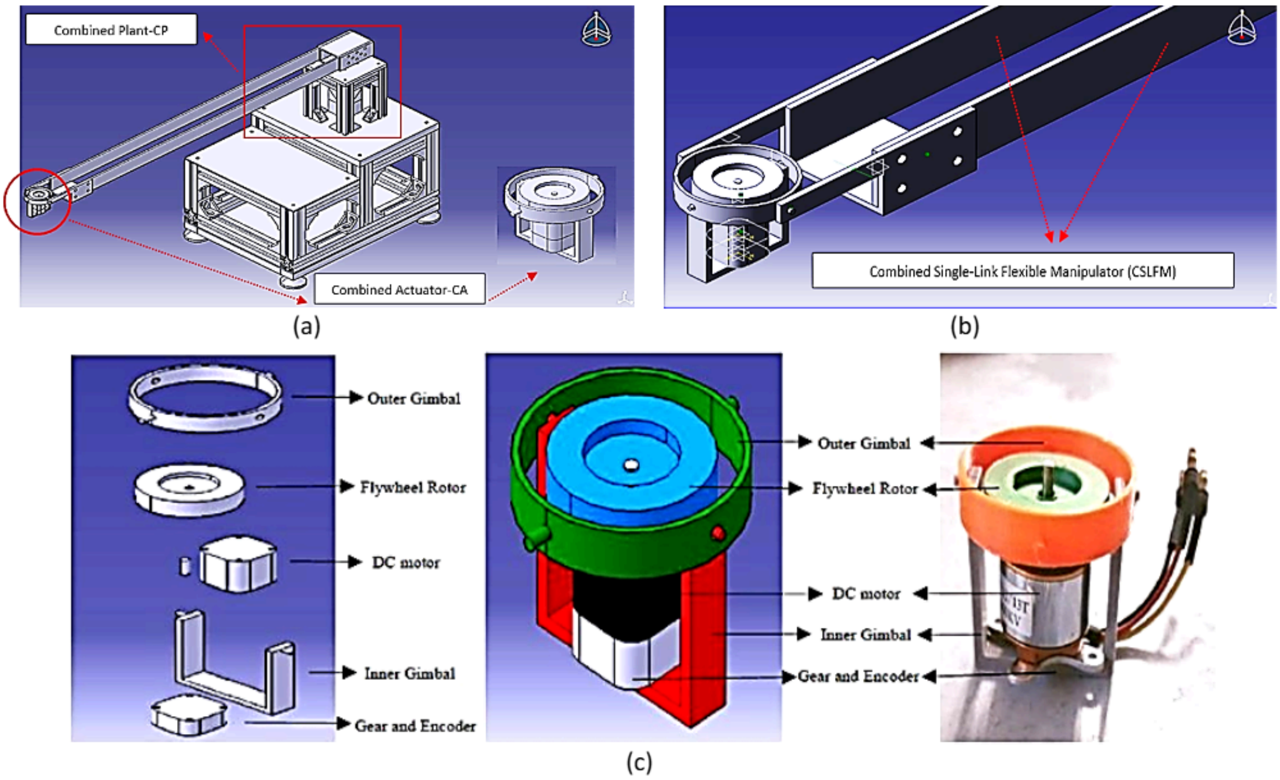

Fig. 4. The front, top, right side, and isometric view of the MTRS (a) MTRS and CA (b) CA and CSLRFM in MTRS (c) Design of the CA

2.4 Experimental National Instruments Set Up

National Instruments (NI) myRIO is a versatile and compact hardware platform designed for students, educators, and engineers to learn and develop applications across various fields, including robotics, mechatronics, and control systems. It combines a real-time processor, a Field-Programmable Gate Array (FPGA), and a suite of input/output (I/O) options within a single device. Below is a description of a typical experimental setup using the NI myRIO.

2.4.1 Hardware components

The NI myRIO device, available in models like myRIO-1900 and myRIO-1950, serves as the core of this setup, chosen based on project needs. A Windows or macOS computer with LabVIEW and myRIO software is essential for programming and interfacing. Some myRIO models require an external power supply with specified voltage and amperage. Various sensors (e.g., temperature, pressure) and actuators (e.g., motors) allow interaction with the environment, and necessary cables connect these components to the myRIO's I/O ports.

2.4.2 Software components

LabVIEW is a graphical programming environment commonly used to develop applications for the myRIO device, supporting control algorithms and user interfaces. The NI myRIO Toolkit complements this by providing LabVIEW libraries and functions specifically for myRIO, making development more efficient.

2.4.3 Experimental set up

To set up the myRIO device, begin by connecting it to your computer via a USB cable, ensuring that all necessary drivers and software are properly installed. If required, attach an external power supply to the myRIO model. Based on the experiment's needs, connect sensors and actuators to the appropriate I/O ports on the myRIO, referring to the documentation for accurate pin configurations. Launch LabVIEW and create a new project, using LabVIEW's graphical programming to develop control algorithms and user interfaces as needed. After completing the program, deploy it to the myRIO device and run the experiment, monitoring data, and controlling actuators from the computer. LabVIEW’s tools also enable logging and analysis of experimental data for thorough data recording and review. Conduct the experiment, collect data, and iteratively refine control algorithms or setup parameters to achieve optimal results.

2.5 Experimental Implementation of MTRS

The experimental views of MTRS and peripherals are shown in Figure 5.

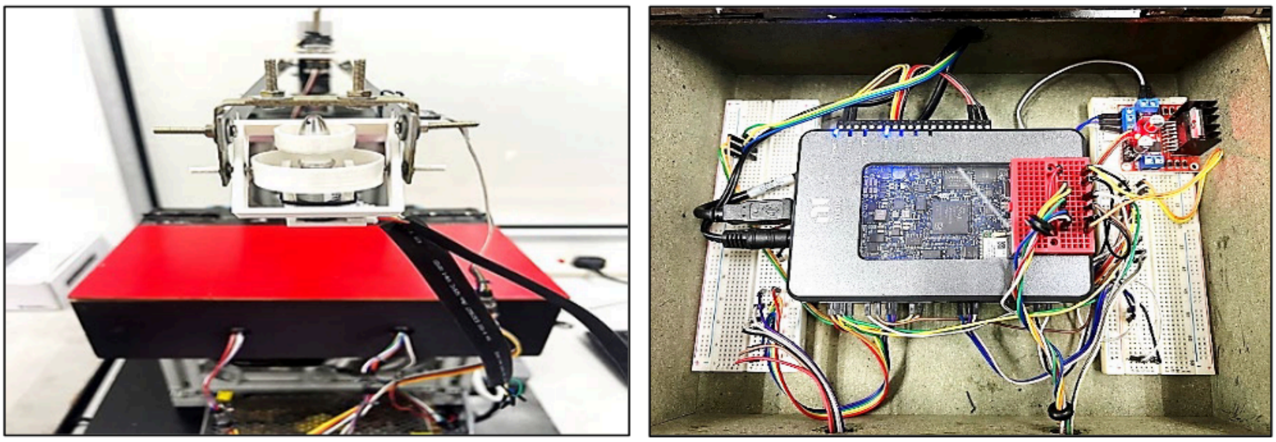

(a) (b)

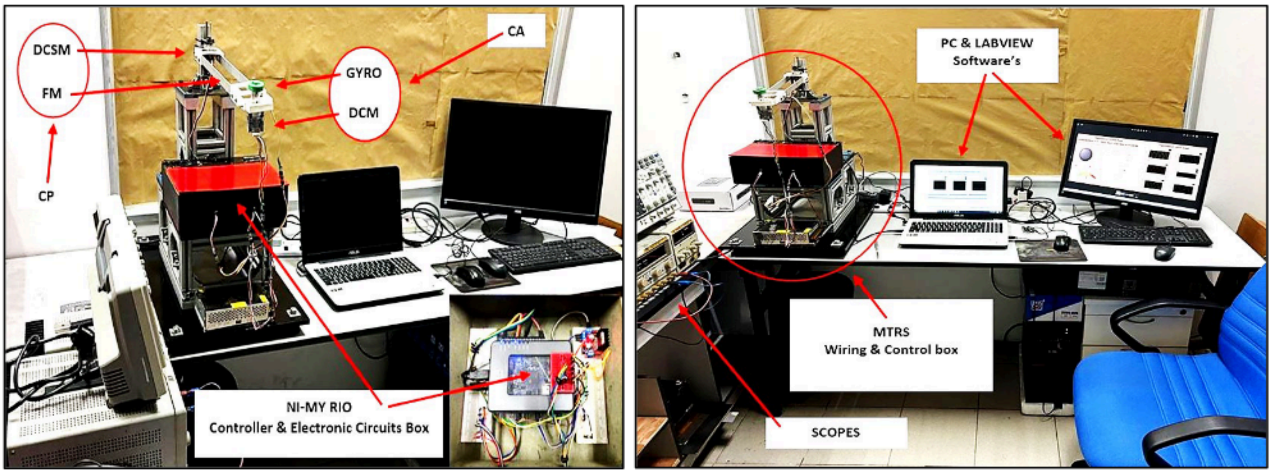

(c) (d)

Fig. 5. The views of mechatronics design and development of MTRS (a) CA (b) NI-myRIO controller (c) Real experimental view of the MTRS (d) Real experimental view of the MTRS peripherals

3. Results and Discussion

3.1 MATLAB Simulation of MTRS with (AVC-DEO-PID) Controller Design

The (AVC-DEO-PID) control design and simulation results for the Multi-Variable Time Response System (MTRS) have been conducted. To evaluate the performance of a Single Link Robotics Flexible Manipulator Model (SLRFMM), Differential Evolution Optimization (DEO) simulations of a closed-loop system model with a PID controller were created in continuous time, as illustrated in Figure 6.

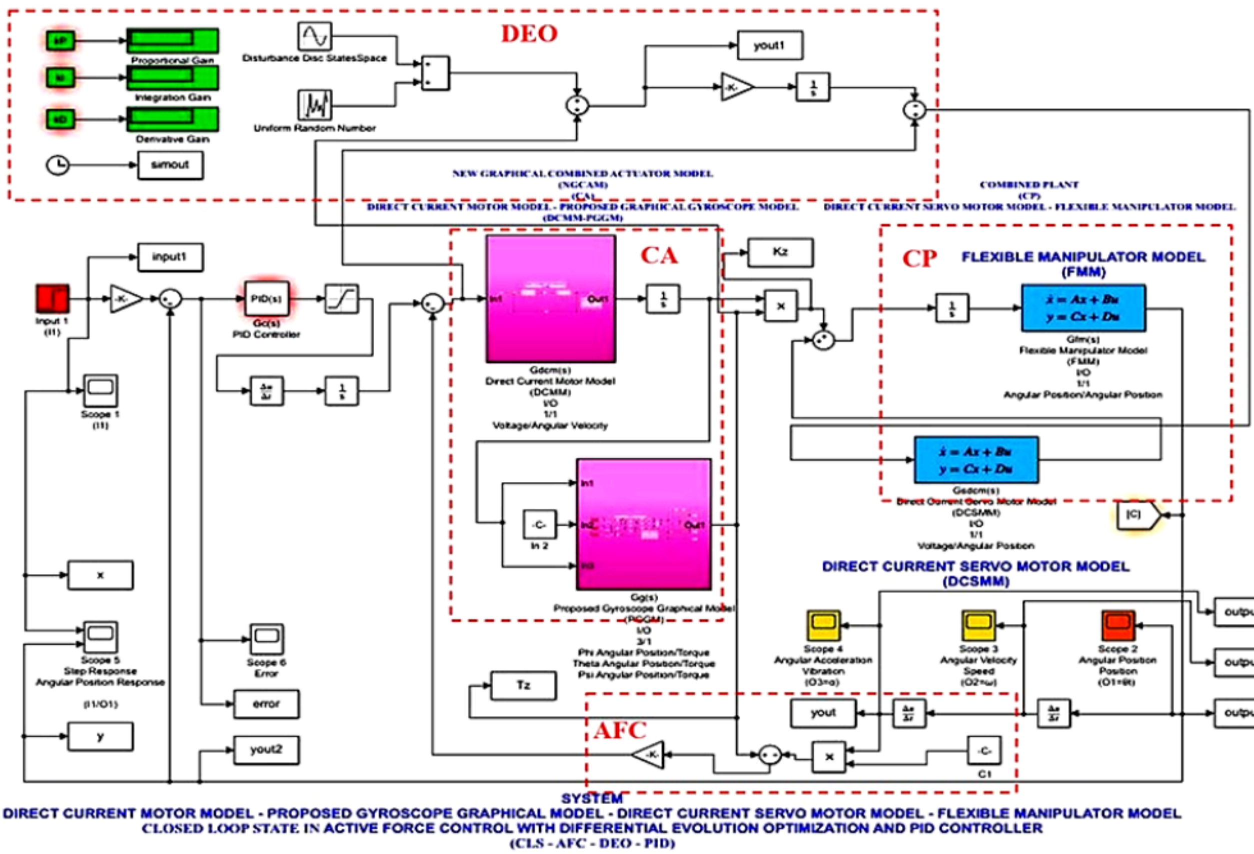

Fig. 6. The (AVC-DEO-PID) control block diagram simulation of MTRS

3.1.1 Simulation run tests comparison

Optimization run tests and a comparative analysis of these tests are shown in Figure 7, with system optimization parameters detailed in Tables 1 through 4. Differential Evolution (DE) strategies are critical for stochastic global optimization, which is sensitive to control parameters and strongly impacts DE performance. As a population-based metaheuristic, DE offers a structured approach for deriving numerical solutions to optimization problems.

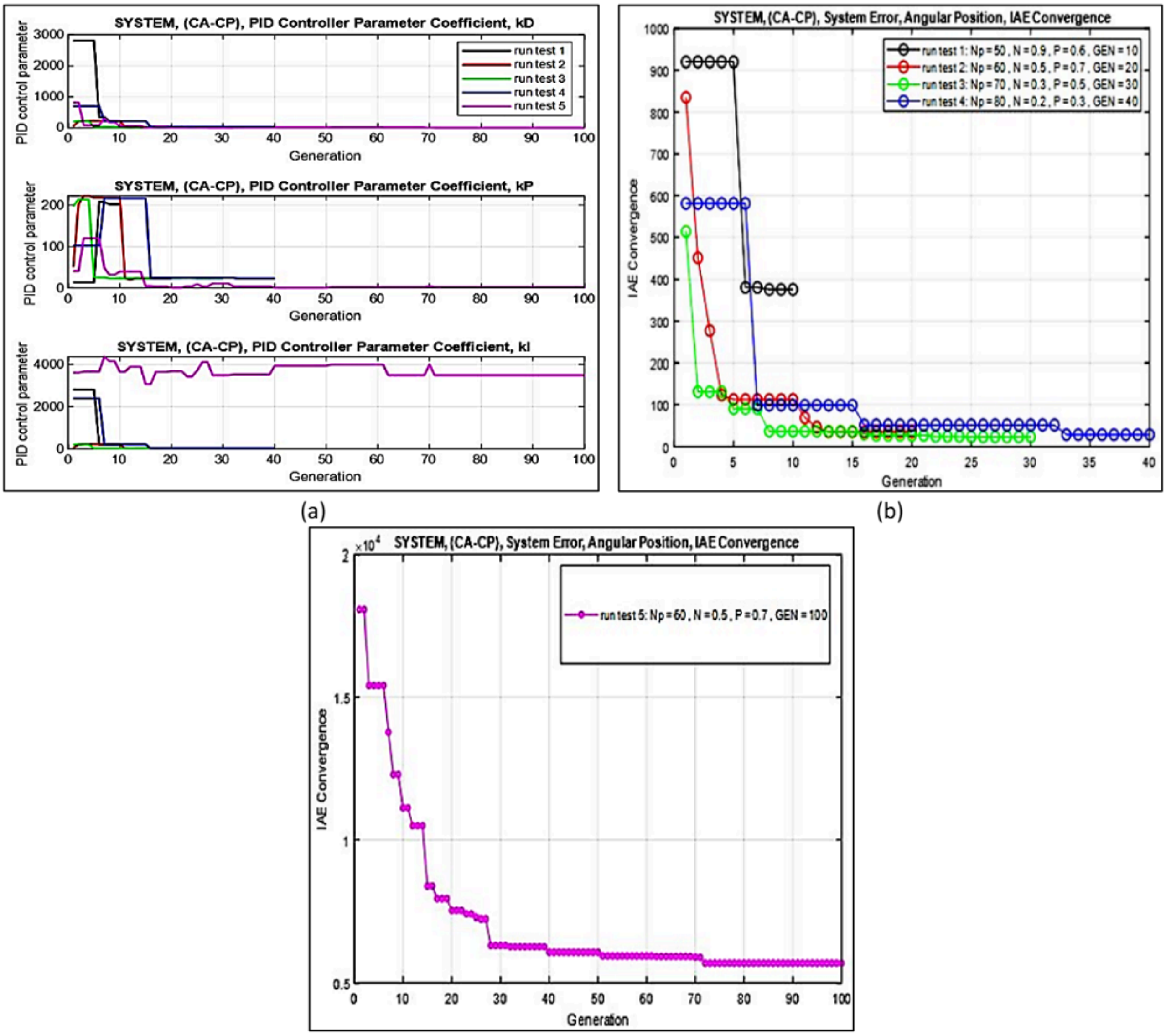

(c)

Fig. 7. The optimization run tests comparison results on MTRS (a) Run test 1 to 5 (b) IAE convergence run tests result in view 2 (c) IAE Convergence and error of run test 5

In Figure 7, the trials demonstrate the consistency of optimal parameters. The algorithm's effectiveness on the system was evaluated based on the Integral of Absolute Error (IAE) criterion, providing a measure of the control performance. In this study, the DE algorithm was executed independently 30 times on the system to facilitate a comparative analysis across runs and to determine the average DE output performance. The influence of population size (N_P), differential weight (N), and crossover (C_R) as (ŋ) was analysed by evaluating all control parameter combinations, with problem dimension (D) also considered. The differential weight range was set from 0.1 to 3, the crossover ranges from 0.1 to 3, the population size from 50 to 100, and the generation count from

10 to 100. Like other evolutionary algorithms, DE outputs are probabilistic, contributing to the variability in results, as indicated in Figures 6 and 7, and in Tables 1 through 4.

The statements in the first column of Table 2 define 5 run tests of MDEAO in experimental, for each 30 times as repetition test to get confirmation to represents the process or conditions for each test. It would be helpful to explain what each "Run Test" corresponds to, whether it refers to the number of iterations, different test scenarios, or distinct conditions under which the test is performed. It would be beneficial to provide more context on the testing process, including what variables are changing across different runs and how the results are calculated. This would give a clearer understanding of the data presented in Table 2.

Table 1
Tuned parameters coefficients of AVC-DEO-PID controller of MTRS

MTRS parameters	Unit	Description	(AVC-DEO-PID)
K_P	Cte.	Proportional	0.4539
K_I	Cte.	Integrator	1.8310
K_D	Cte.	Derivative	3481.2
N	Cte.	Cte.	75.0000

Table 2
DEO coefficients of MTRS

Run test	I_{best}	F_{best}	Time
Run Test 1-30 times	19	1151.6	475.2258
Run Test 2-30 times	39	2341.98	1063.8
Run Test 3-30 times	25	1518.21	1818.4
Run Test 4-30 times	69	4034.58	2756.5
Run Test 5-30 times	36	600	777.6

Table 3 presents PID controller tuning parameters and DEO coefficients across different run tests each in 30 times, highlighting variations in population size, differential weight, crossover rates, and generations. Results indicate that as the number of generations increases, the parameter ranges narrow, suggesting finer control system tuning. Whereas, Table 4 shows PID controller parameters (k_P, k_I, k_D) tuned via DEO in different tests. Most coefficients exhibit minor variations, while Run Test 5 shows significantly diverging values, indicating unique tuning with a high number of generations.

Table 3
PID controller tuned parameters and DEO coefficients of MTRS

Run Test	Population size	Differential weight		Crossover		Generation
RT	N_P	N_{min}	N_{max}	η_{min}	η_{max}	GEN
Run Test 1	50	0.1	1.7	0.3	0.9	10
Run Test 2	60	0.4	0.6	0.5	0.9	20
Run Test 3	70	0.1	0.5	0.2	0.8	30
Run Test 4	80	0.1	0.3	0.1	0.5	40
Run Test 5	60	0.1	0.9	0.6	0.8	100

Table 4
PID controller tuned parameters and DEO coefficients of MTRS

Run Test	Population size	Generation	DEO coefficients		
RT	N_P	GEN	k_P	k_I	k_D
Run Test 1	50	10	44.0332	44.0332	44.0332
Run Test 2	60	20	23.0551	23.0551	23.0551
Run Test 3	70	30	23.0284	23.0284	23.0284
Run Test 4	80	40	22.7323	22.7323	22.7323
Run Test 5	60	100	0.4539	1.8310	3481.2

3.1.2 Simulation performance evaluation of MTRS

Figure 8 shows the simulation performance evaluation of the MTRS results. Here, the angular position and error performance of the MTRS are evaluated using different controllers. It is clear that the (AFC-DEO-PID) controller outperforms the others, with output 1 closely tracking input 1.

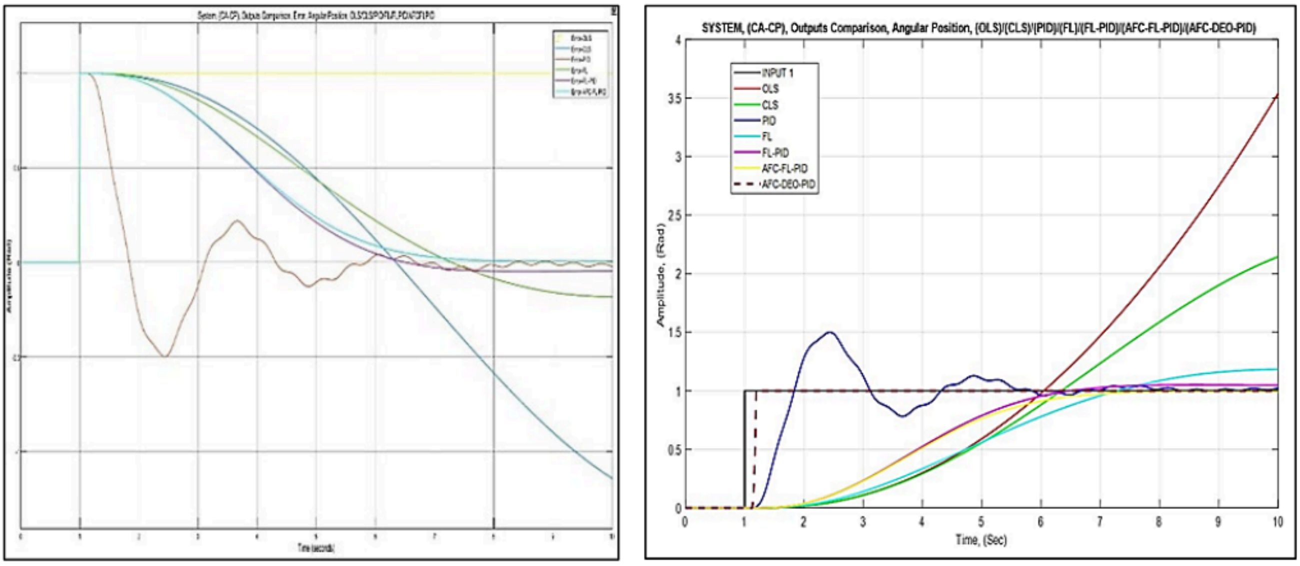

(a) (b)

Fig. 8. The simulation performance evaluation of MTRS signal graph results and unit step response (a) Error-angular position (b) Angular position

3.2 LABVIEW Experimental of MTRS with (AVC-DEO-PID) Controller Design

Experimental control, results, and data analysis are essential components of any scientific experiment or research project. This section presents the LABVIEW and NI-MYRIO experimental control, results, and data analysis of MTRS. The specific techniques and tools used for experimental control, data collection, and analysis are determined by the field of study and the nature of the experiment. Figures 9 and 10 illustrate the experimental panels, wiring diagrams, and results as detailed below.

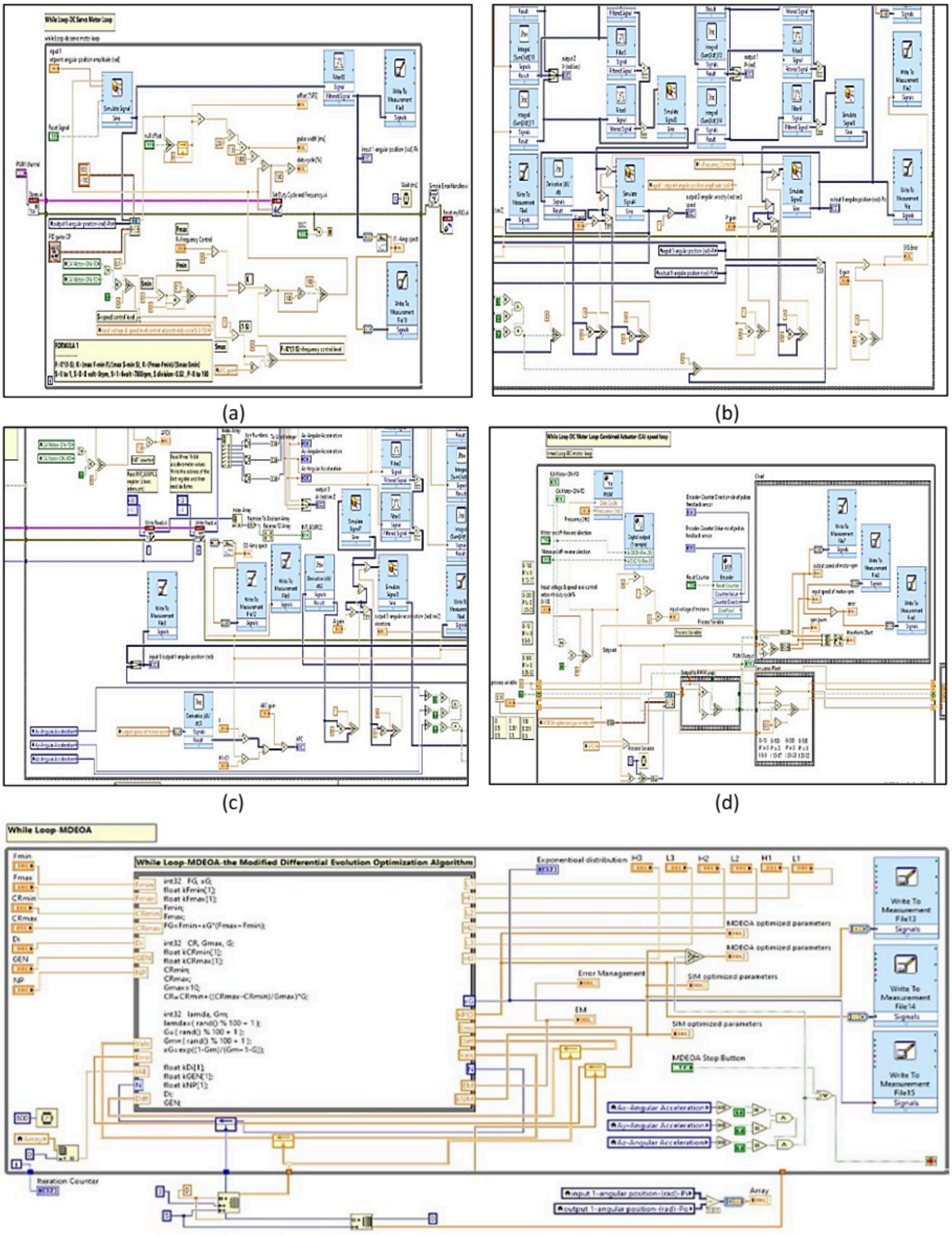

(e)

Fig. 9. LABVIEW experimental wiring diagrams and loops of MTRS with AVC-DEO-PID controller (a) DC servo motor loop in CP (b) ACC. sensor loop 1 (c) ACC. sensor loop 2 (d) DC motor loop in CA (e) MDEOA loop wiring

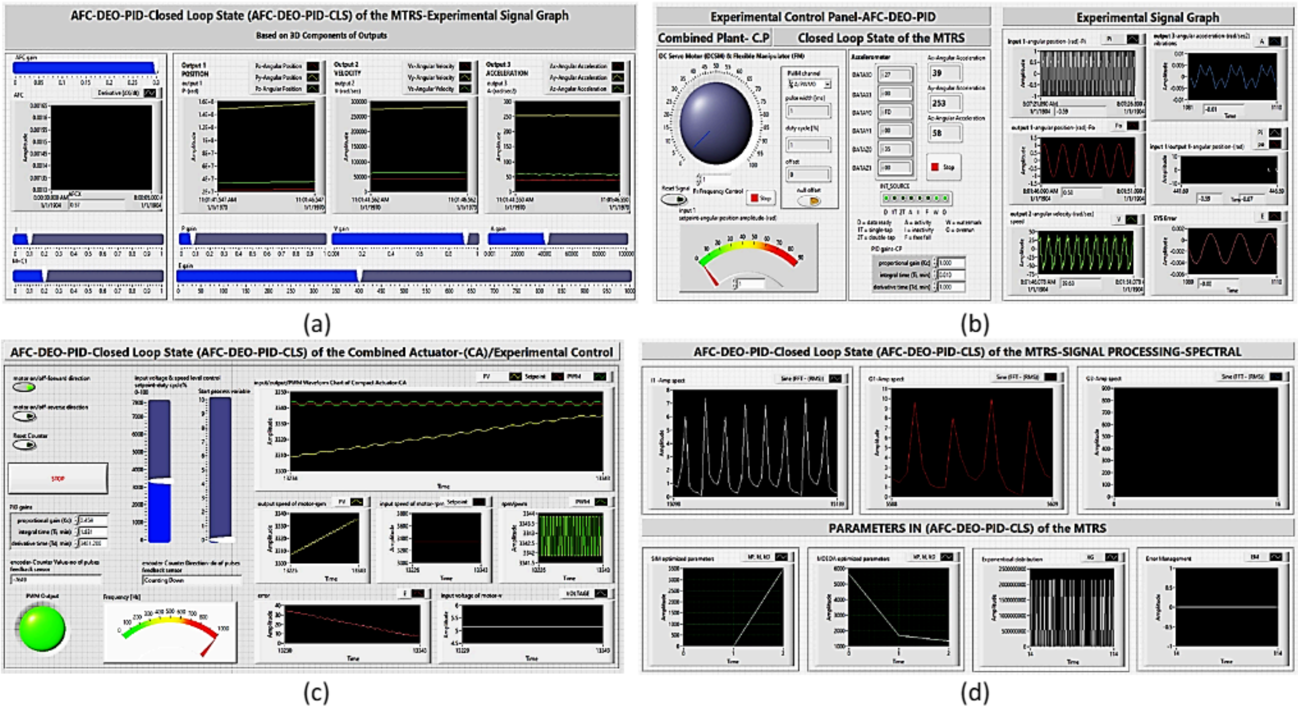

Fig. 10. LABVIEW experimental control panels of MTRS with (AVC-DEO-PID) controller (a) Gains control (b) DC servo motor loop in CP (c) DC motor loop in CA (d) Signal spectral

3.2.1 Experimental run tests comparison
3.2.1.1 Output 1-angular position

Figure 11 shows the angular position as output 1 in experimental tests under different system conditions and controllers. The best performance is achieved with the (CLS-AFC-DEO-PID) controller, which tracks the input very well.

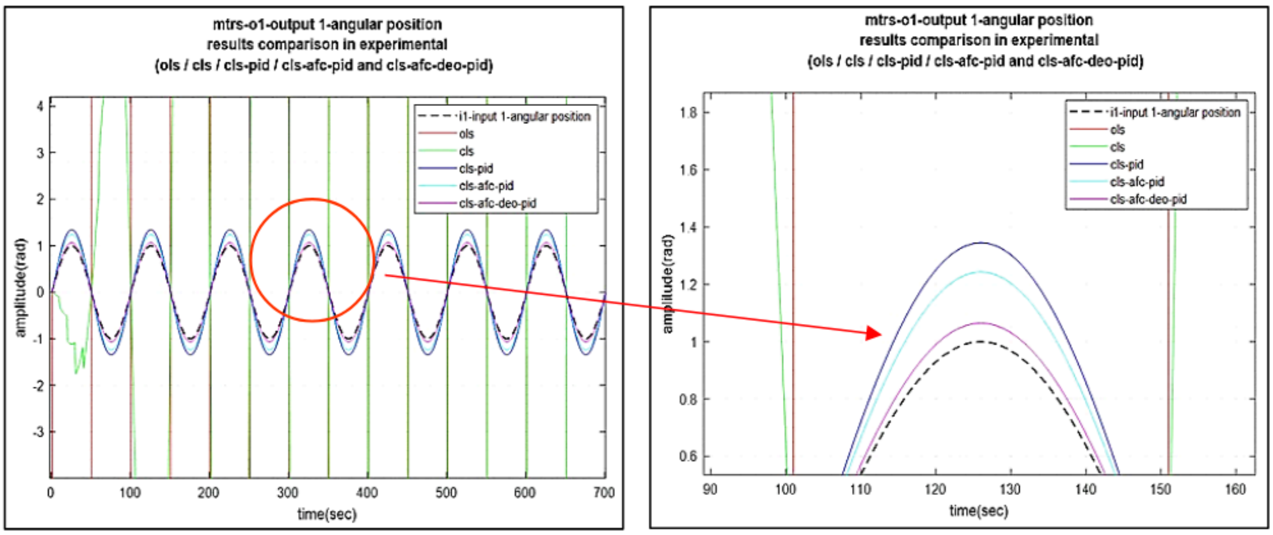

Fig. 11. Experimental angular position results comparison of output 1

3.2.1.2 Output 3-angular acceleration

Figure 12 displays the angular acceleration (vibration) as output 3 in experimental tests. The (CLS-AFC-DEO-PID) controller effectively reduces vibration to zero, meeting the target of minimizing vibrations.

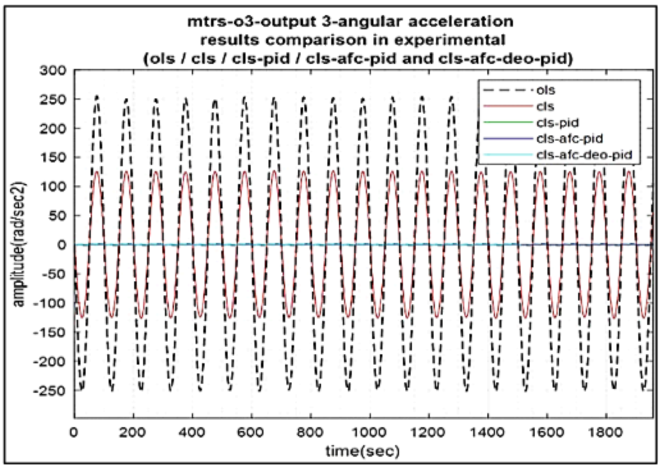

(a)

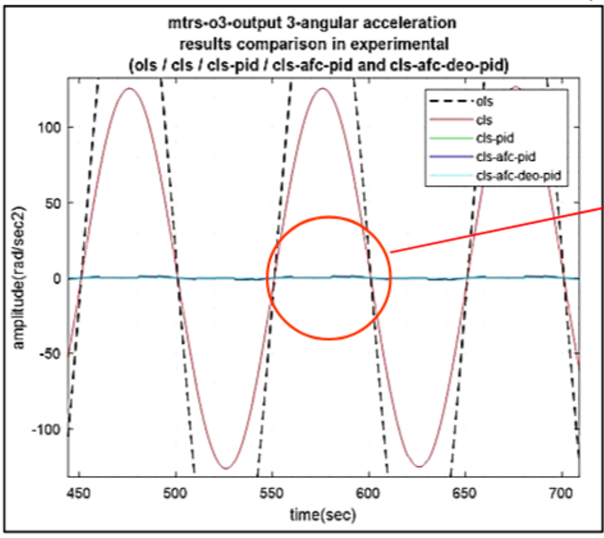

(b)

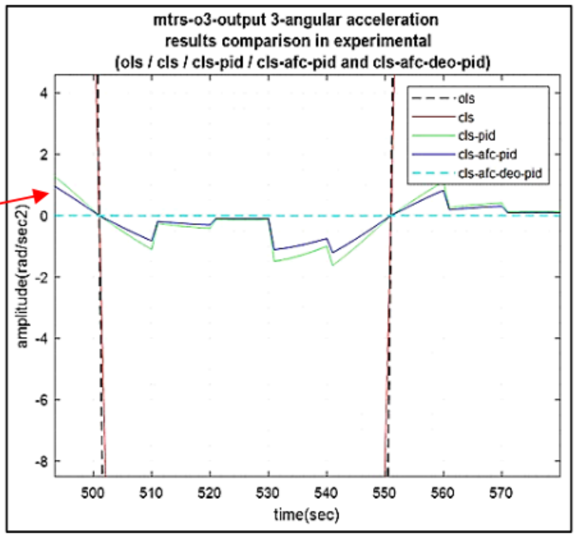

(c)

Fig. 12. Experimental angular acceleration results comparison of output 3 (a) Angular acceleration (b) and (c) Angular acceleration amplitude-vibration

3.2.1.3 Output 1 frequency

This Figure 13 compares and shows the frequency response of angular position in a multi-variable time response system (MTRS) under various control strategies. The x-axis represents frequency (660–760 Hz), and the y-axis shows amplitude (radians). The open-loop system shows the highest resonance, while advanced controllers like "cls-afc-deo-pid" significantly reduce vibrations, demonstrating superior performance.

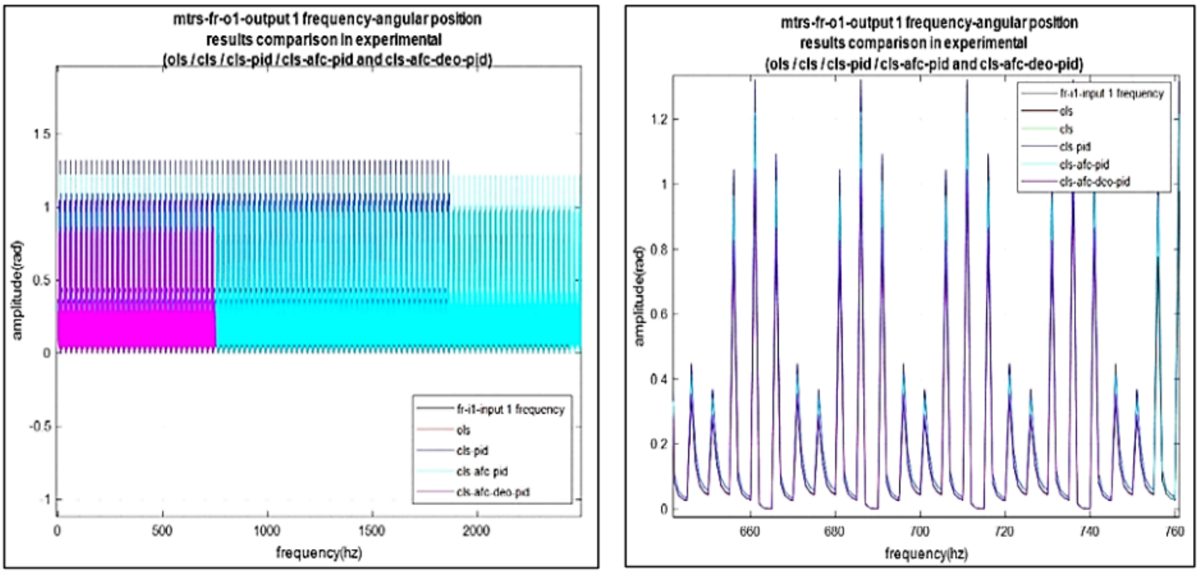

Fig. 13. Experimental frequency results comparison of output 1

3.2.1.4 Output 3 frequency

This Figure 14 shows the frequency response of angular acceleration for a multi-variable time response system (MTRS) under different control strategies. The x-axis represents frequency (950–1150 Hz), and the y-axis shows the amplitude of angular acceleration (rad/s²). The legend compares all configurations. The open-loop system exhibits the highest resonance peaks, while closed-loop controllers progressively reduce the amplitude. "Cls-afc-deo-pid" demonstrates the most significant vibration suppression, minimizing acceleration peaks and showcasing its effectiveness in controlling high-frequency vibrations.

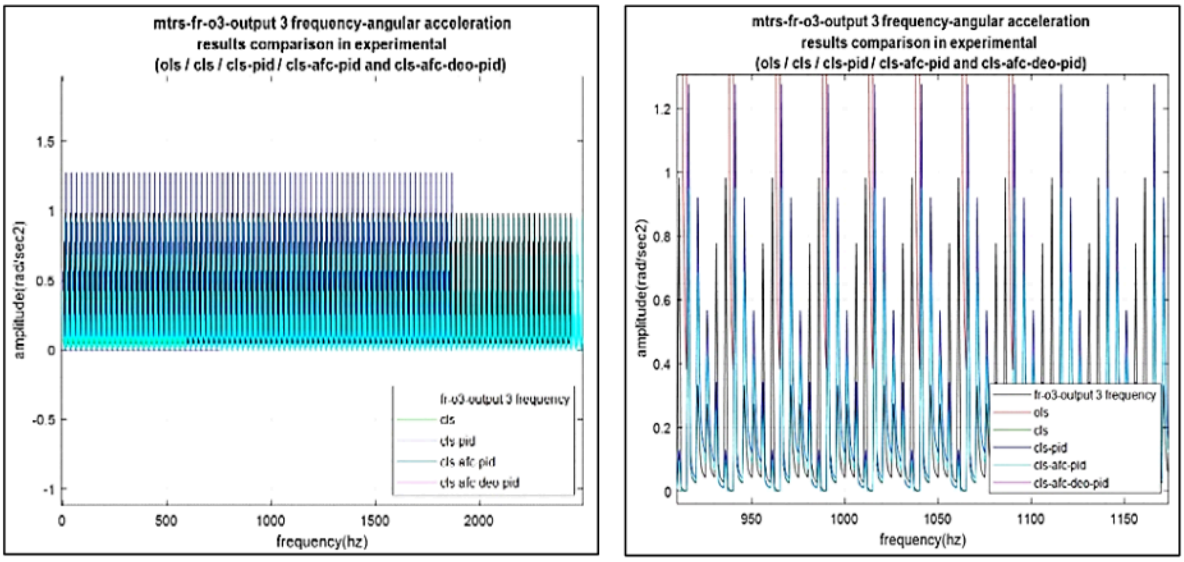

Fig. 14. Experimental frequency results comparison of output 3

3.2.1.5 System error

Figures 15(a) and 15(b) show the system's angular position error in experimental tests under various controllers. The (CLS-AFC-DEO-PID) controller reduces error to zero, ensuring the system output accurately tracks the input. Sections c, d, and e illustrate the input and output speeds of the DC motor in the Combined Actuator (CA) under different controllers, highlighting the effect on voltage and speed error.

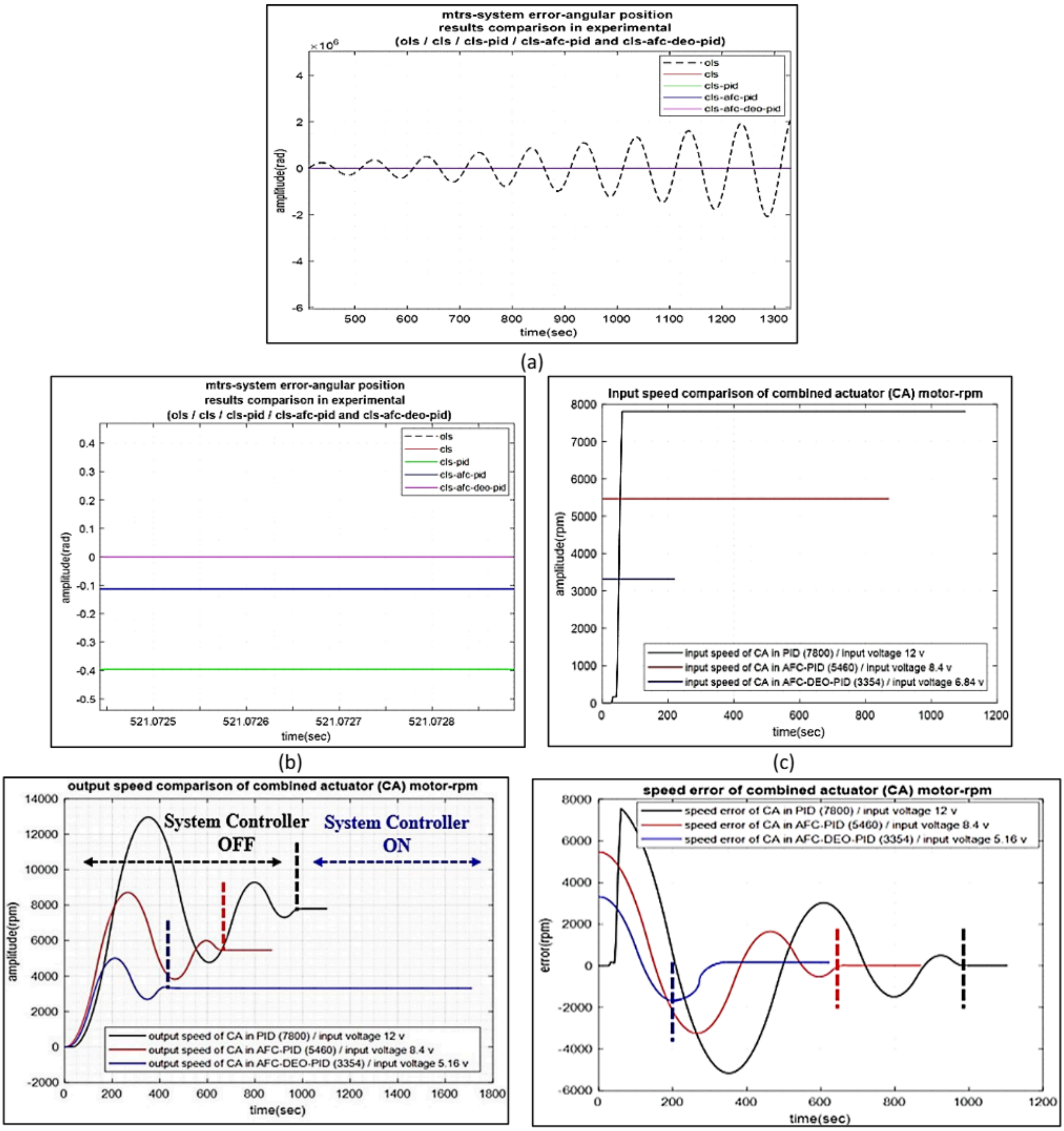

Fig. 15. Experimental error results comparison of system-MTRS (a) System error: Angular position amplitude view 1 (b) System error: Angular position amplitude view 2 (c) Input speed comparison (d) Output speed comparison (e) Speed error comparison

3.3 Evaluating of Controllers in Simulation and Experimental
3.3.1 Simulation evaluating of controllers vs PID

Table 5 compares simulation results for angular position input ($I_1=\theta_i$) across PID, (AVC-PID), and (AVC-DEO-PID) controllers, indicating identical performance metrics. This suggests all controllers achieve consistent amplitude, frequency, phase, and time response parameters in simulation. Figure 16 presents the same angular position input applied to the system in a simulation test for further comparisons.

Table 5
Controller's parameters vs input 1-angular position in simulation

MTRS parameters: Input 1-angular position ($I_1=\theta_i$)		PID simulation	(AVC-PID) simulation	(AVC-DEO-PID) simulation
1	A_{mp}	1.000 rad	1.000 rad	1.000 rad
2	F_{req}	1.000 Hz	1.000 Hz	1.000 Hz
3	P_h	0.000 rad	0.000 rad	0.000 rad
4	R_{ms}	0.707	0.707	0.707
5	T_R	1.008 s	1.008 s	1.008 s
6	T_P	1.578 s	1.578 s	1.578 s
7	T_S	1.578 s	1.578 s	1.578 s
8	M_P	0.000 rad	0.000 rad	0.000 rad

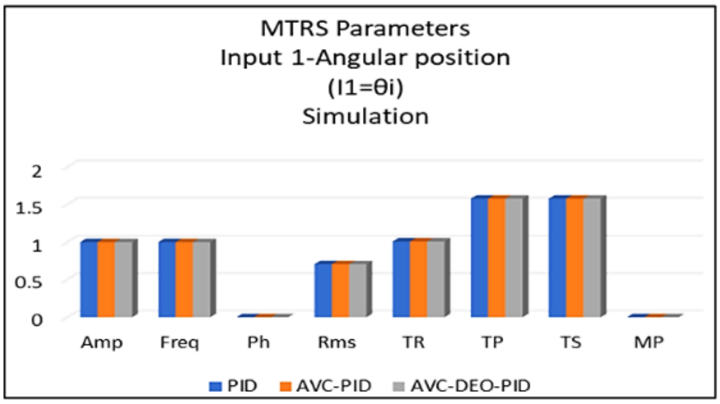

Fig. 16. Controller's comparison vs input 1-angular position in SIM

Table 6 highlights output angular position ($O_1=\theta_t$) performance across controllers, with (AVC-DEO-PID) showing superior damping (lowest amplitude, RMS, and overshoot) and faster settling time (T_S = 1.001 s), indicating enhanced precision and stability.

Table 6
Controller's parameters vs output 1-angular position in SIM

MTRS parameters: Output 1-angular position ($O_1=\theta_t$)		PID simulation	(AVC-PID) simulation	(AVC-DEO-PID) simulation
1	A_{mp}	1.294 rad	1.196 rad	1.000 rad
2	F_{req}	1.294 Hz	1.196 Hz	1.000 Hz
3	P_h	180 rad	180 rad	0.000 rad
4	R_{ms}	0.914	0.845	0.707
5	T_R	1.002 s	1.800 s	0.9 s
6	T_P	2.008 s	2.001 s	1.01 s
7	T_S	15.332 s	12.334 s	1.001 s
8	M_P	0.294 rad	0.196 rad	0.00 rad

Figure 17 illustrates the angular position as output 1 in the simulation test, showing that the (AVC-DEO-PID) controller outperforms others in parameters like amplitude, frequency, rise time, peak time, settling time, and maximum overshoot.

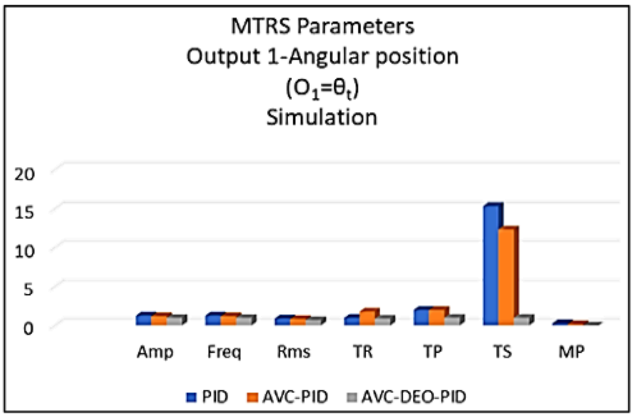

Fig. 17. Controller's comparison vs output 1-angular position in SIM

Table 7 shows that for angular acceleration ($O_3=\alpha$), (AVC-DEO-PID) completely suppresses oscillations (Amplitude, Frequency, RMS = 0), demonstrating superior control performance. Its higher tuning parameters (K_I, K_D) contribute to precise and stable results compared to PID and (AVC-PID). Figure 18 demonstrates the angular acceleration as output 3 in the simulation test, where the (AVC-DEO-PID) controller achieves the lowest values in system parameters such as amplitude, frequency, and steady-state error.

Table 7
Controller's parameters vs output 3-angular acceleration in SIM

MTRS parameters: Output 3-angular acceleration ($O_3=\alpha$)		PID simulation	(AVC-PID) simulation	(AVC-DEO-PID) simulation
1	A_{mp}	1.902 rad/s^2	1.530 rad/s^2	0.000 rad/s^2
2	F_{req}	1.902 Hz	1.530 Hz	0.000 Hz
3	R_{ms}	1.344	1.081	0.000
4	K_P	1.985	1.985	0.4539
5	K_I	0.026	0.026	1.8310
6	K_D	33.590	33.590	3481.2
7	N	257.242	257.242	75.0000
8	E_{SS}	0.467 rad	0.437 rad	0.000 rad

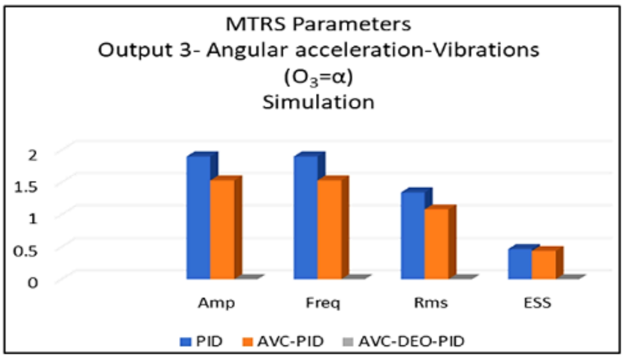

Fig. 18. Controller's comparison vs output 3-angular acceleration in SIM

Figure 19(a) compares the performance of the (AVC-DEO-PID) and (AVC-PID) controllers against the PID controller in simulation. Section (b) shows the percentage effectiveness of the (AVC-DEO-PID) controller in performance compared to the PID controller. The (AVC-PID) controller shows a notable improvement over the PID controller in several performance metrics. The (TR) coefficient increased by 79.640%, leading to a slower system response. However, (TP) and (TS) coefficients were optimized by 0.348% and 24.306%, respectively, resulting in faster response times. The (MP) coefficient increased by 33.333%, causing system overshoot and instability, while the ESS coefficient was optimized by 6.423%, enhancing system responsiveness.

In addition, the (AVC-DEO-PID) controller displayed even more significant improvements compared to the PID controller. The (TR) coefficient decreased by 10.179%, slightly slowing the response, while (TP) and (TS) coefficients were optimized by 49.701% and 93.471%, respectively, resulting in a much faster response. Notably, (MP) and (ESS) coefficients were optimized by 100%, ensuring a stable, overshoot-free, and highly responsive system. In comparison, the (AVC-DEO-PID) controller achieved a 70.670% optimization in vibration control and stabilization, whereas the (AVC-PID) controller showed a 16.102% improvement. These results highlight the (AVC-DEO-PID) controller's superior stabilization and vibration control over the other systems.

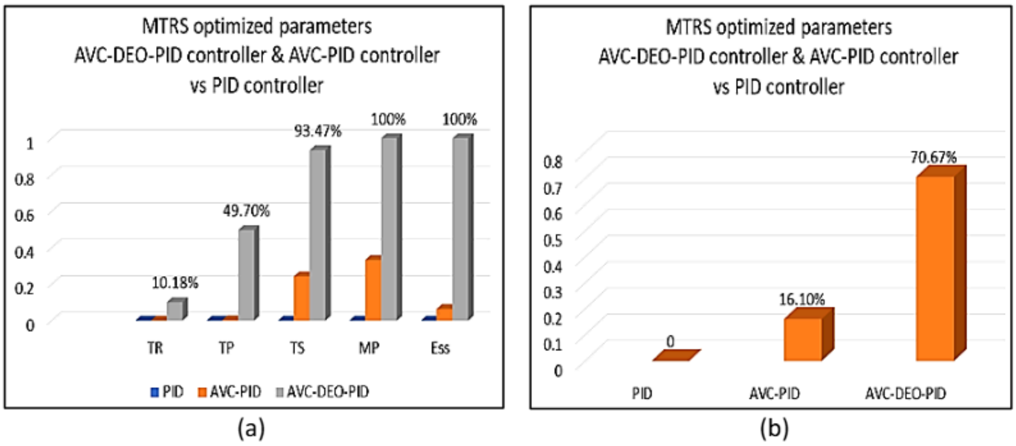

Fig. 19. MTRS optimized parameters AVC-DEO-PID controller and AVC-PID controller vs PID controller in SIM (a) Parameter's comparison (b) Controllers' comparison

3.3.2 Experimental evaluating of controllers vs PID

Figure 20 shows the angular position as output 1 in the experimental test under different controllers for further comparisons.

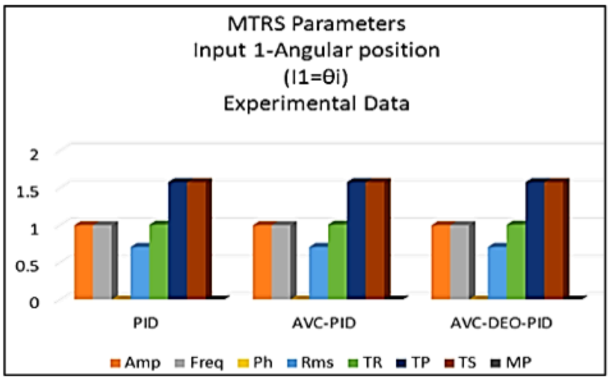

Fig. 20. Controller's comparison vs input 1-angular position in EXP

Tables 8 and 9, shows that the (AVC-DEO-PID) controller outperforms PID and (AVC-PID), achieving the lowest amplitude, fastest rise time, shortest settling time, and zero overshoot for angular position. For angular acceleration, it completely suppresses vibrations, reduces RMS to zero, and eliminates steady-state error, making it the most precise and stable controller for MTRS systems.

Table 8
Controller's parameters vs output 1-angular position in EXP

MTRS parameters: Output 1-angular position (O_1=θ_t)		PID experimental	(AVC-PID) experimental	(AVC-DEO-PID) experimental
1	A_{mp}	1.30794 rad	1.20896 rad	1.000 rad
2	F_{req}	1.30794 Hz	1.20896 Hz	1.000 Hz
3	P_h	180.00000 rad	180.00000 rad	0.000 rad
4	R_{ms}	0.92471	0.85473	0.707
5	T_R	1.01202 s	1.26800 s	0.9 s
6	T_P	2.02808 s	1.57501 s	1.01 s
7	T_S	15.48532 s	12.45734 s	1.001 s
8	M_P	0.30794 rad	0.20896 rad	0.00 rad

Table 9
Controller's parameters vs output 3-angular acceleration in EXP

MTRS parameters: Output 3-angular acceleration (O_3= α)		PID experimental	(AVC-PID) experimental	(AVC-DEO-PID) experimental
1	A_{mp}	1.30010 rad/s^2	1.23130 rad/s^2	0.000 rad/s^2
2	F_{req}	1.30010 Hz	1.23130 Hz	0.000 Hz
3	R_{ms}	0.91917	0.87052	0.000
4	K_P	1.985	1.985	0.4539
5	K_I	0.026	0.026	1.8310
6	K_D	33.590	33.590	3481.2
7	N	257.242	257.242	75.0000
8	E_{SS}	0.47167 rad	0.44137 rad	0.000 rad

Figure 21 displays the angular position as output 1 in the experimental test, with the (AVC-DEO-PID) controller again showing superior performance in controller parameters. Figure 22 illustrates the angular acceleration as output 3 in the experimental test, where the (AVC-DEO-PID) controller excels in minimizing steady-state error.

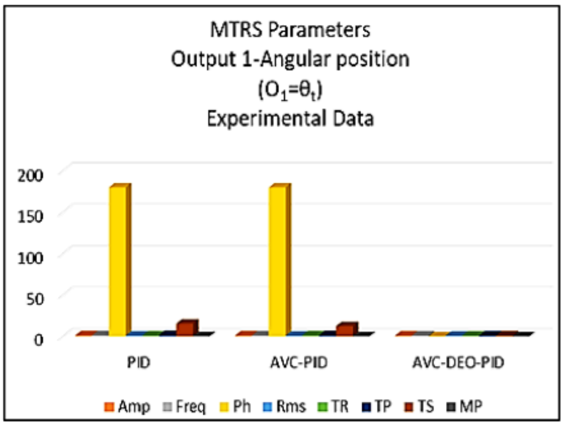

Fig. 21. Controller's comparison vs output 1 angular position in EXP

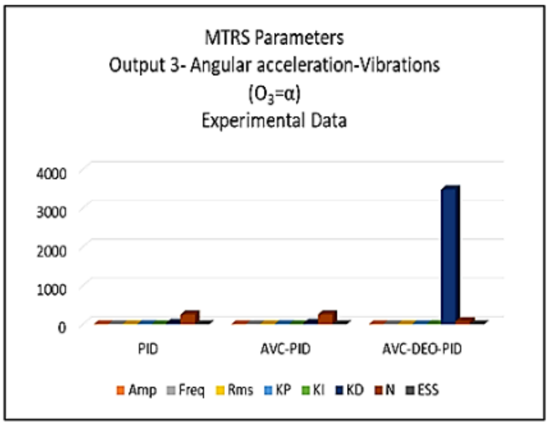

Fig. 22. Controller's comparison vs output 3 Angular acceleration in EXP

3.3.3 Evaluating of controller's strategies

Figure 23(a) compares the optimized (AVC-DEO-PID) controller with the (AVC-PID) and PID controllers in experimental tests, showing the best performance with (AVC-DEO-PID). Section (b) demonstrates the effectiveness of (AVC-DEO-PID) compared to the PID controller. In the (AVC-PID) controller compared to the PID controller, the Transient Response (T_R) coefficient increased by 25.293%, resulting in a slower system response. The Peak Time (T_P) coefficient was optimized by 22.339%, enabling a faster system response. The Settling Time (T_S) coefficient saw a 19.553% optimization, further enhancing response speed. However, the Maximum Peak (M_P) coefficient increased by 32.142%, indicating overshoot and reduced stability. The Steady-State Error (E_{SS}) coefficient was optimized by 6.423%, improving system responsiveness.

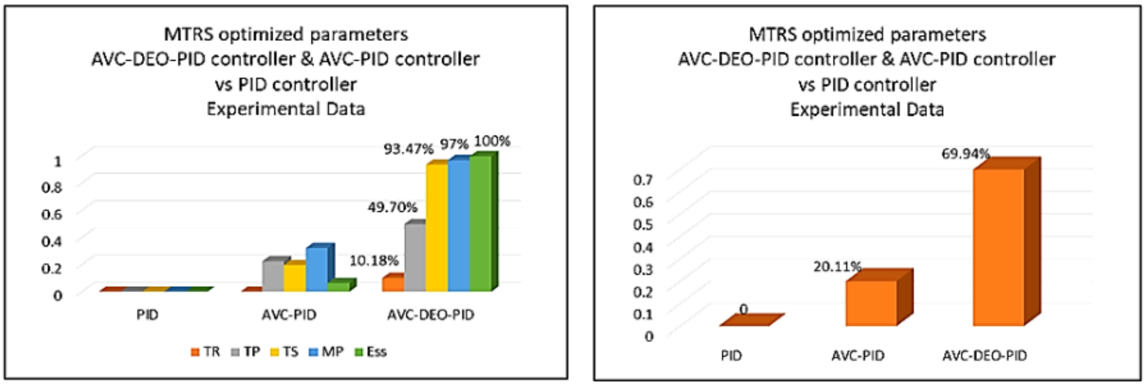

(a) (b)

Fig. 23. MTRS optimized parameters (AVC-DEO-PID) controller and (AVC-PID) controller vs PID controller in EXP (a) Parameter's comparison (b) Controllers' comparison

For the (AVC-DEO-PID) controller relative to the PID controller, the (T_R) coefficient decreased by 10.179%, slowing response time. The (T_P) coefficient was optimized by 49.701%, and the (T_S) coefficient by 93.471%, both significantly increasing response speed. The (M_P) coefficient was optimized by 96.752%, eliminating overshoot and enhancing stability. Additionally, the (E_{SS}) coefficient improved by 99.575%, resulting in the best responsive conditions. The (AVC-DEO-PID) controller achieved a 69.935% overall optimization, while the (AVC-PID) controller reached 20.114%, showing significant stabilization and vibration control compared to other systems. This analysis highlights the superior stabilization and vibration control performance of the (AVC-DEO-PID) controller. Table 10 shows performance improvements in simulation and experimental setups. (AVC-DEO-PID) outperforms PID by ~70%, while (AVC-PID) achieves moderate improvements (~16-20%), highlighting (AVC-DEO-PID0 as the most effective controller.

Table 10
MTRS controller's comparison in SIM and EXP

Controller comparison	Simulation	Experimental
(AVC-DEO-PID) vs (PID) controller	70.670 %	69.935 %
(AVC-PID) vs (PID) controller	16.102 %	20.114 %

Table 11 compares system errors, with (AVC-DEO-PID) achieving near-zero error in both simulation and experimental setups, while PID and (AVC-PID) exhibit higher errors. OLS/CLS methods yield significantly larger errors, underscoring (AVC-DEO-PID's) superior accuracy. Figure 24 evaluates the effectiveness of different controllers in both simulation and experimental tests, clearly showing that the (AVC-DEO-PID) controller outperforms the (AVC-PID) and PID controllers. Figure 25 compares the system error in simulation and experimental tests, demonstrating that the (AVC-DEO-PID) controller minimizes error better than the (AVC-PID) and PID controllers.

Table 11
MTRS system error's comparison in SIM and EXP

MTRS	OLS	CLS	PID	(AVC-PID)	(AVC-DEO-PID)
Error in simulation	4000000	20000	0.467	0.437	0.000
Error in experimental	4000000	20000	0.47167	0.44137	0.002

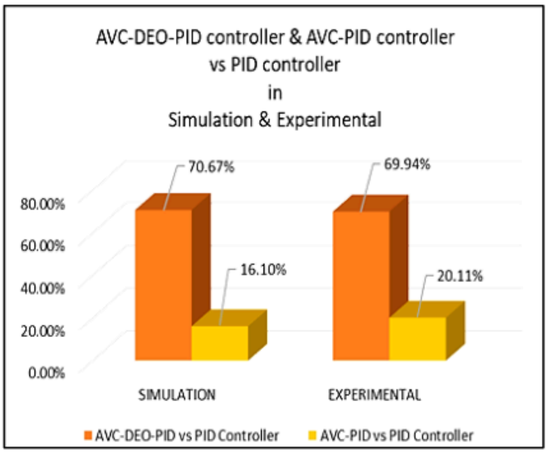

Fig. 24. MTRS controller's comparison in SIM and EXP

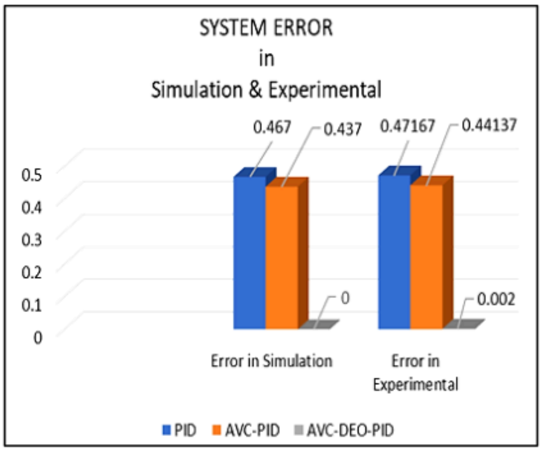

Fig. 25. MTRS system error's comparison in SIM and EXP

Table 12 shows minimal differences between simulation and experimental results for (AVC-DEO-PID), with consistent low percentage deviations (1% or less) and zero phase and overshoot error, demonstrating superior consistency compared to PID and (AVC-PID).

Table 12
Controller's parameters comparison in SIM and EXP

MTRS parameters	Exp vs SIM in (PID)	Exp vs SIM in (AVC-PID)	Exp vs SIM in (AVC-DEO-PID)
A_{mp}	1.08%	1.08%	1%
F_{req}	1.08%	1.08%	1%
P_h	0%	0%	0%
R_{ms}	1.17%	1.15%	1%
T_R	1.00%	-29.56%	1%
T_P	1.00%	-21.28%	1%
T_S	1.00%	1.00%	1.00%
M_P	4.75%	6.61%	0%

Figure 26 presents the percentage changes in experimental vs simulation parameters, indicating that the (AVC-DEO-PID) controller balances system parameters more effectively than the others. Table 13 demonstrates that (AVC-DEO-PID) outperforms all other controllers across different system states, achieving minimal amplitude and frequency in outputs (O_1, O_2, O_3) and near-zero error (0.002 rad). It also reduces acceleration in (NGCA), confirming its superior precision and efficiency.

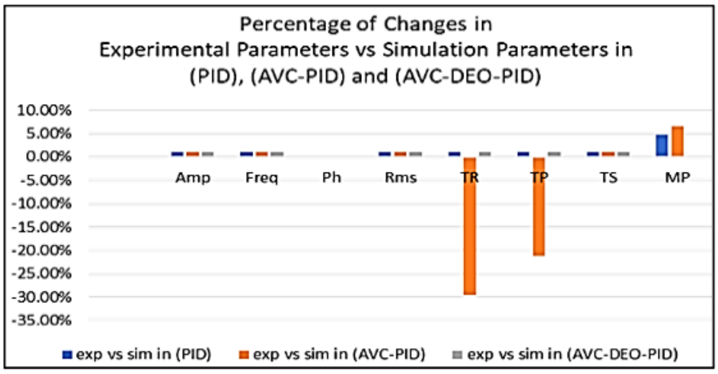

Fig. 26. Percentage of changes of controller's parameters in SIM and EXP

Table 13
Controller's criteria's parameters in system's different states

MTRS parameters definition	OLS exp	CLS exp	PID exp	(AVC-PID) exp	(AVC-DEO-PID) exp
(I_1-Amp)	1.000 rad	1.000 rad	1.000 rad	1.000 rad	1.000 rad
(O_1-Amp)	4000000 rad	20000 rad	1.30794 rad	1.20896 rad	1.010 rad
(O_2-Amp)	50000 rad/s	100 rad/s	130 rad/s	150 rad/s	50 rad/s
(O_3-Amp)	250 rad/s^2	130 rad/s^2	1.30010 rad/s^2	1.23130 rad/s^2	0.005 rad rad/s^2
(E_{rr})	4000000 rad	20000 rad	0.47167 rad	0.44137 rad	0.002 rad
(I_1- Freq)	1.000 Hz	1.000 Hz	1.000 Hz	1.000 Hz	1.000 Hz
(O_1- Freq)	4000000 Hz	20000 Hz	1.30794 Hz	1.20896 Hz	1.010 Hz
(O_3- Freq)	250 Hz	130 Hz	1.30010 Hz	1.23130 Hz	0.005 Hz
(S_i-NGCA)	0 rpm	0 rpm	7800 rpm	5460 rpm	3354 rpm
(S_o- NGCA)	0 rpm	0 rpm	7800 rpm	5460 rpm	3354 rpm
(S_{er}- NGCA)	0 rpm	0 rpm	0 rpm	0 rpm	0 rpm

3.4 Validation

Compare the controllers PID, (AVC-FL-PID), (AVC-DEO-PID), and Ref 2 and 3 in system output in parameters T_R, T_P, T_S, M_P, and E_{SS} and with unit step function as system input.

3.4.1 Validation in simulation

Table 14 compares the performance of various controllers for angular position output with a unit step input. (AVC-DEO-PID) shows the best performance with the lowest values for overshoot (M_P), steady-state error (E_SS), and settling time (T_S), indicating superior efficiency and stability. Figure 27 shows the angular position as output 1 and evaluates the performance of different controllers in simulation, confirming that the (AVC-DEO-PID) controller balances system parameters best.

Table 14
Simulation parameters comparison in controllers in system for output 1-angular position with unit step function as system input

MTRS parameters	PID	(AVC-FL-PID)	(AVC-DEO-PID)	Ref 2	Ref 3
T_R	1.7546	5.0549	1.5760	1.1570	4.0700
T_P	2.5324	5.9254	1.2738	1.5000	5.2720
T_S	5.8510	5.6079	0.3820	2.1850	10.7000
M_P	0.5324	0.3074	0.0	1.5000	0.8190
E_{SS}	0.0200	0.0093	0.0	0.0298	0.0982

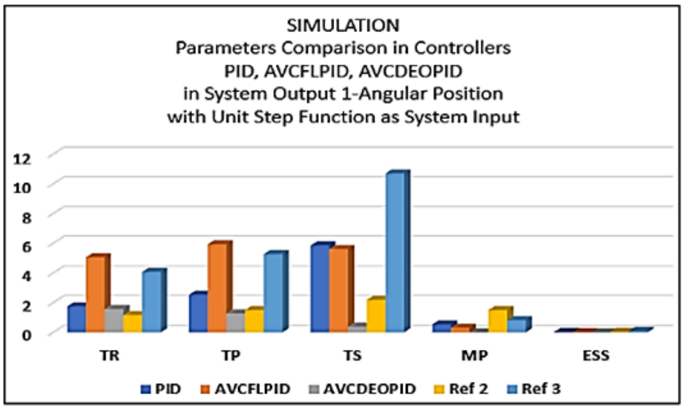

Fig. 27. Simulation parameters comparison in controllers in system for output 1-angular position

Figure 28 displays the angular position as output 1 with a sine input in the simulation, highlighting the (AVC-DEO-PID) controller's superior performance in balancing system parameters. Table 15 highlights the superior performance of (AVC-DEO-PID) over PID in response to a sine wave input, achieving lower rise time (T_R), peak time (T_P), settling time (T_S), overshoot (M_P), and steady-state error (E_{SS}), indicating better precision and faster stabilization.

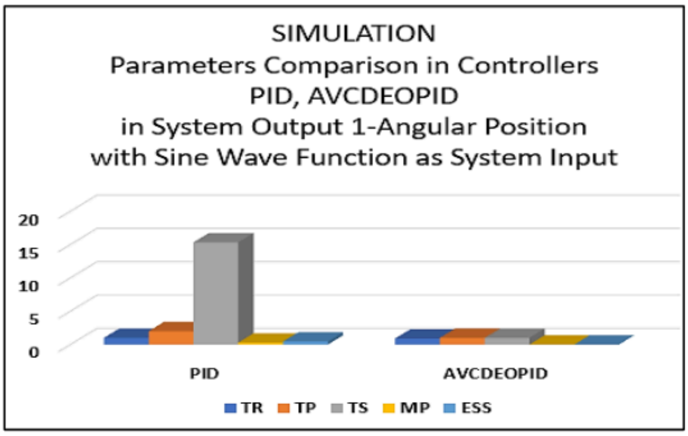

Fig. 28. Simulation parameters comparison in controllers in system for output 1-angular position with sine

Table 15
Simulation parameters comparison in controllers in system for output 1-angular position with sine wave function as system input

MTRS parameters	PID	AVCDEOPID
T_R	1.002	0.9
T_P	2.008	1.01
T_S	15.332	1.001
M_P	0.294	0.00
E_{SS}	0.467	0.000

3.4.2 Validation in experimental

Table 16 shows that in the experimental setup, (AVC-DEO-PID) outperforms PID in all parameters for angular position output with a sine wave input. It demonstrates faster rise time (T_R), peak time (T_P), and settling time (T_S), with zero overshoot (M_P) and steady-state error (E_{SS}), indicating superior accuracy and stability. Whereas, Table 17 demonstrates that (AVC-DEO-PID) achieves identical performance in both simulation and experimental setups, with zero overshoot (M_P) and steady-state error (E_{SS}), and consistent rise time (T_R), peak time (T_P), and settling time (T_S), confirming its robustness and accuracy across both conditions.

Table 16
Experimental parameters comparison in controllers in system for output 1-angular position with sine wave function as system input

MTRS parameters	PID	AVCDEOPID
T_R	1.01202	0.9
T_P	2.02808	1.01
T_S	15.48532	1.001
M_P	0.30794	0.00
E_{SS}	0.47167	0.000

Table 17
Parameters comparison in controllers AVCDEOPID in system for output 1-angular position with sine wave function as system input

MTRS parameters	SIM	EXP
T_R	0.9	0.9
T_P	1.01	1.01
T_S	1.001	1.001
M_P	0.00	0.00
E_{SS}	0.000	0.000

Figure 29 shows the same input (sine) in the experimental test, where the (AVC-DEO-PID) controller again outperforms other controllers. Figure 30 compares angular position as output 1 across different system parameters in simulation and experimental tests, demonstrating minimal difference between the two. Figure 31 compares angular acceleration (vibrations) across controllers in MTRS for both simulation and experimental tests, showing that the (AVC-DEO-PID) controller performs the best in both conditions.

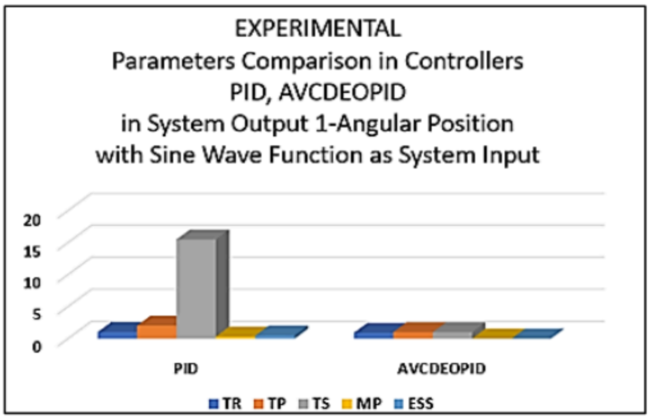

Fig. 29. Experimental parameters comparison in controllers in system for output 1 angular position with sine wave

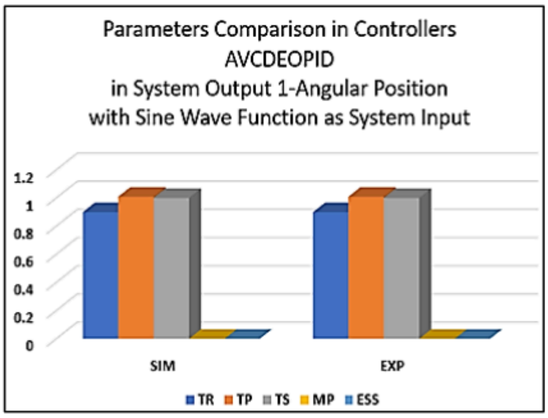

Fig. 30. Parameters comparison in controllers AVCDEOPID in system for output 1 angular position with sine wave

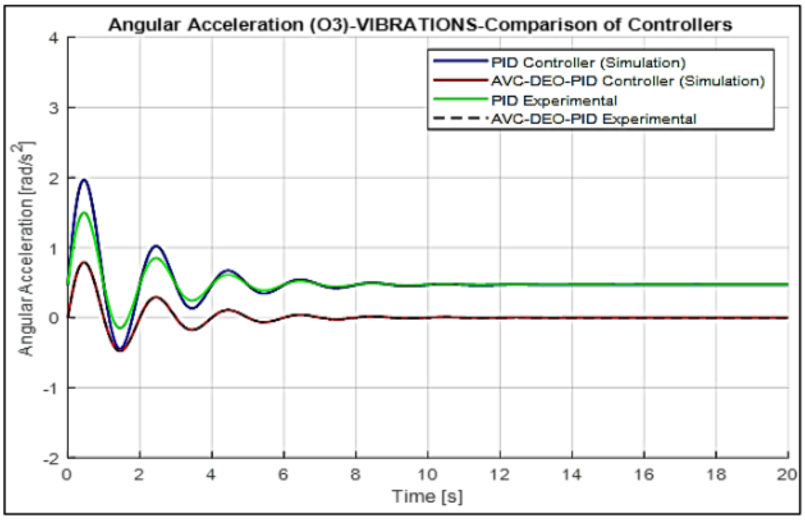

Fig. 31. Angular acceleration (vibrations) comparison of controllers in MTRS

4. Conclusions and Discussion

This research successfully developed a dynamic Mechatronics Test Rig System (MTRS) and introduced advanced control strategies for Robotic Flexible Manipulators (RFM), focusing on the Combined Single-Link Robotics Flexible Manipulator (CSLRFM). Through MATLAB simulations and LABVIEW experimental control, multiple models including the Flexible Manipulator Model (FMM), Direct Current Servo Motor Model (DCSMM), Combined Plant (CP), Gyroscope Graphical Model (GGM) with Euler Angles Φ (Phi), Θ (Theta) and ψ(Psi), Proposed Gyroscope Graphical Model (PGGM), and New Graphical Combined Actuator Model (NGCAM) were analysed. The study utilized a Modified Differential Evolution Optimization Algorithm (MDEOA) to optimize PID controllers, integrated with the New Gyroscopic Combined Actuator (NGCA) for Intelligent Active Vibration Control (IAVC). Results demonstrated that the (AVC-DE-PID) and (AVC-FL-PID) controllers significantly outperformed traditional methods, providing enhanced stabilization and vibration suppression.

Simulation and experimental findings, validated and verified using LABVIEW and NI-MYRIO, confirmed the robustness of the proposed strategies in real-time scenarios. Additionally, data analysis and comparative evaluations of control algorithms, including those for the Direct Current Motor Model (DCMM) and MTRS, underscored the importance of innovative control methods. These methods eliminate the need for extensive prior controller design knowledge while achieving superior performance. This research offers essential insights into RFM dynamics and establishes a foundation for future applications in mechatronics and robotics. The findings highlight the critical role of advanced control algorithms in improving performance for complex dynamic systems.

Acknowledgements
The authors would like to thank Universiti Putra Malaysia (UPM) and the Malaysian Ministry of Higher Education (MOHE) for their continuous support in the research work. This work was supported in part by the Geran Putra Inisiatif (GPI) fund (GPI/2024/9794100).

References
[1] Kelly, S. Graham. *Mechanical vibrations: Theory and applications*. Nelson Education, 2011.
[2] Tokhi, M. Osman, Z. Mohamed, and M. Hasan Shaheed. "Dynamic characterisation of a flexible manipulator system." *Robotica* 19, no. 5 (2001): 571-580. https://doi.org/10.1017/S0263574700003209

[3] Readman, Mark, and Pierre Bélanger. "Acceleration feedback for flexible joint robots." In *Proceedings of the 30th IEEE Conference on Decision and Control* p. 1385-1390. 1991. https://doi.org/10.1109/CDC.1991.261627

[4] Li, Hong-Xing, and CL Philip Chen. "The equivalence between fuzzy logic systems and feedforward neural networks." *IEEE Transactions on Neural Networks* 11, no. 2 (2000): 356-365. https://doi.org/10.1109/72.839006

[5] Abdulameer, Ashwaq, Marizan Sulaiman, Mohd Shahrieel Mohd Aras, and Dawood Saleem. "Tuning methods of PID controller for DC motor speed control." *Indonesian Journal of Electrical Engineering and Computer Science* 3, no. 2 (2016): 343-349. https://doi.org/10.11591/ijeecs.v3.i2.pp343-349

[6] Bankar, Vishal Kiran, and A. S. Aradhye. "A review on active, semi-active and passive vibration damping." *International Journal of Current Engineering and Technology* 6, no. 10.1155 (2016): 2019.

[7] Miljković, Dubravko. "Review of active vibration control." *32nd Information and Communication Technology, Electronics and Microelectronics* (2009): 103-108.

[8] Bailey, Thomas, and James E. Hubbard Jr. "Distributed piezoelectric-polymer active vibration control of a cantilever beam." *Journal of Guidance, Control, and Dynamics* 8, no. 5 (1985): 605-611. https://doi.org/10.2514/3.20029

[9] Storn, Rainer, and Kenneth Price. "Differential evolution–a simple and efficient heuristic for global optimization over continuous spaces." *Journal of Global Optimization* 11 (1997): 341-359. https://doi.org/10.1023/A:1008202821328

[10] Qin, A. Kai, Vicky Ling Huang, and Ponnuthurai N. Suganthan. "Differential evolution algorithm with strategy adaptation for global numerical optimization." *IEEE Transactions on Evolutionary Computation* 13, no. 2 (2008): 398-417. https://doi.org/10.1109/TEVC.2008.927706

[11] Rehman, Muhammad Zia Ur, Roman Kalvin, Muhammad Zain Ul Abideen, Muhammad Waqas Mustafa, and Juntakan Taweekun. "Implementation of EFI System in 70cc Bike." *Semarak Engineering Journal* 6, no.1 (2024):1-10. https://doi.org/10.37934/sej.6.1.110

[12] Alhaji, Ibrahim Abubakar, Zulkifly Abbas, and Aliyu Sisa Aminu. "Experimental and simulated investigation of s-parameters and power loss characteristics of PTFE/glass composites at X-band frequency." *Malaysian Journal on Composites Science and Manufacturing* 15, no. 1 (2024): 1-12. https://doi.org/10.37934/mjcsm.15.1.112

[13] Moloody, Abbas, Azizan As'arry, Tang Sai Hong, Raja Kamil, and Ali Zolfagharian. "PID controller parameter tuning based on a modified differential evolutionary optimization algorithm for the intelligent active vibration control of a combined single link robotics flexible manipulator." *Journal of Advanced Research in Applied Sciences and Engineering Technology* 52, no. 1 (2025): 234-258. https://doi.org/10.37934/araset.52.1.234258

[14] Moloody, Abbas, Azizan As'arry, Tang Sai Hong, Raja Kamil, and Irfan Bahiuddin. "Analysis, modelling and simulation for the intelligent active vibration control of a combined plant using a new gyroscopic combined actuator model." *Journal of Advanced Research in Applied Sciences and Engineering Technology* 63, no. 1 (2026): 102–129. https://doi.org/10.37934/araset.63.1.102129

[15] Gol Zardian, Mohsen, and Amran Ayob. "Intelligent modelling and active vibration control of flexible manipulator system." *Journal of Vibroengineering* 17, no. 4 (2015): 1879-1891.

[16] Sastry, Shankar. *Nonlinear systems: analysis, stability, and control*. Vol. 10. Springer Science & Business Media, 2013.

[17] Shi, Shenghao, Dongxu Li, and Qing Luo. "Design and dynamic analysis of micro-vibration isolator for Single Gimbal Control Moment Gyro." *Procedia Engineering* 99 (2015): 551-559. https://doi.org/10.1016/j.proeng.2014.12570

[18] Mohamed, Ali Wagdy, and Abdulaziz S. Almazyad. "Differential evolution with novel mutation and adaptive crossover strategies for solving large scale global optimization problems." *Applied Computational Intelligence and Soft Computing* 2017, no. 1 (2017): 7974218. https://doi.org/10.1155/2017/7974218

[19] Rahman, TA Zahidi, and IZ Mat Darus. "Active vibration control of a flexible plate via active force control strategy." In *2011 4th International Conference on Mechatronics (ICOM)*, p. 1-6. IEEE, 2011. https://doi.org/10.1109/ICOM.2011.5937194

[20] Rajeswari, K., and P. Lakshmi. "Simulation of suspension system with intelligent active force control." In *2010 International Conference on Advances in Recent Technologies in Communication and Computing*, p. 271-277. IEEE, 2010. https://doi.org/10.1109/ARTCom.2010.21

[21] Moloody, Abbas, Azizan As'arry, Tang Sai Hong, Mohd Sapuan Salit, and Raja Kamil. "Modelling and simulation of the position control of flexible manipulator using gyroscopic actuator." *International Symposium on Applied Sciences and Engineering (ISASE)*, 2021.

[22] Moloody, Abbas, Azizan As' arry, Tang Saihong, Raja Kamil, and Mohd Zuhri Mohamed Yusoff. "A comprehensive review based on analysis modeling, mechanical vibration control strategies, and optimization methods of robotics flexible manipulator structures." *Pertanika Journal of Science & Technology* 33, no. 1 (2025). https://doi.org/10.47836/pjst.33.1.02

[23] Tokhi, Mohammad Osman, and Abul KM Azad. "Design and development of an experimental flexible manipulator system." *Robotica* 15, no. 3 (1997): 283-292. https://doi.org/10.1017/S0263574797000325

[24] Belherazem, A., R. Salim, A. Laidani, and M. Chenafa. "Vibration control of a two-link flexible manipulator." *Automatic Control and Computer Sciences* 58, no. 3 (2024): 346-358. https://doi.org/10.3103/S0146411624550017

[25] Keshtkar, Sajjad, Jaime A. Moreno, Hirohisa Kojima, Kenji Uchiyama, Masahiro Nohmi, and Keisuke Takaya. "Spherical gyroscopic moment stabilizer for attitude control of microsatellites." *Acta Astronautica* 143 (2018): 9-15. https://doi.org/10.1016/j.actaastro.2017.10.033

[26] Deif, Sarah, Mohammad Tawfik, and Hanan A. Kamal. "Optimal tuning of a PD controller for a single-link flexible robot arm using adaptive genetic algorithm." In *International Conference on Aerospace Sciences and Aviation Technology* 14, no. p. 1-11, 2011. https://doi.org/10.21608/asat.2011.23261

[27] John, Subash, Abdul Imran Rasheed, and Viswanath K. Reddy. "ASIC implementation of fuzzy-PID controller for aircraft roll control." In *2013 International Conference on Circuits, Controls and Communications (CCUBE)*, p. 1-6. IEEE, 2013. https://doi.org/10.1109/CCUBE.2013.6718551

[28] Lakshmi, K. Vijaya, and P. Srinivas. "Fuzzy adaptive PID control of pitch system in variable speed wind turbines." In *2014 International Conference on Issues and Challenges in Intelligent Computing Techniques (ICICT)*, p. 52-57. IEEE, 2014. https://doi.org/10.1109/ICICICT.2014.6781252

[29] Jovanović, Miroslav M., Aleksandar M. Simonović, Nemanja D. Zorić, Nebojša S. Lukić, Slobodan N. Stupar, and Slobodan S. Ilić. "Experimental studies on active vibration control of a smart composite beam using a PID controller." *Smart Materials and Structures* 22, no. 11 (2013): 115038. https://doi.org/10.1088/0964-1726/22/11/115038

[30] Hadi, M. Sukri, Intan Z. Mat Darus, M. Osman Tokhi, and Mohd Fairus Jamid. "Active vibration control of a horizontal flexible plate structure using intelligent proportional–integral–derivative controller tuned by fuzzy logic and artificial bee colony algorithm." *Journal of Low Frequency Noise, Vibration and Active Control* 39, no. 4 (2020): 1159-1171. https://doi.org/10.1177/1461348419852454